Winter 1984

SOLAR MODULATION OF GALACTIC COSMIC RAYS: TECHNIQUES & APPLICATIONS (SHOCK ACCELERATION, ANTIPROTONS)

JOHN STEVEN PERKO
University of New Hampshire, Durham

INFORMATION TO USERS

This reproduction was made from a copy of a document sent to us for microfilming. While the most advanced technology has been used to photograph and reproduce this document, the quality of the reproduction is heavily dependent upon the quality of the material submitted.

The following explanation of techniques is provided to help clarify markings or notations which may appear on this reproduction.

1. The sign or "target" for pages apparently lacking from the document photographed is "Missing Page(s)". If it was possible to obtain the missing page(s) or section, they are spliced into the film along with adjacent pages. This may have necessitated cutting through an image and duplicating adjacent pages to assure complete continuity.

2. When an image on the film is obliterated with a round black mark, it is an indication of either blurred copy because of movement during exposure, duplicate copy, or copyrighted materials that should not have been filmed. For blurred pages, a good image of the page can be found in the adjacent frame. If copyrighted materials were deleted, a target note will appear listing the pages in the adjacent frame.

3. When a map, drawing or chart, etc., is part of the material being photographed, a definite method of "sectioning" the material has been followed. It is customary to begin filming at the upper left hand corner of a large sheet and to continue from left to right in equal sections with small overlaps. If necessary, sectioning is continued again—beginning below the first row and continuing on until complete.

4. For illustrations that cannot be satisfactorily reproduced by xerographic means, photographic prints can be purchased at additional cost and inserted into your xerographic copy. These prints are available upon request from the Dissertations Customer Services Department.

5. Some pages in any document may have indistinct print. In all cases the best available copy has been filmed.

University
Microfilms
International

300 N. Zeeb Road
Ann Arbor, MI 48106

Perko, John Steven

SOLAR MODULATION OF GALACTIC COSMIC RAYS: TECHNIQUES & APPLICATIONS

University of New Hampshire PH.D. 1984

PLEASE NOTE:

In all cases this material has been filmed in the best possible way from the available copy. Problems encountered with this document have been identified here with a check mark _✓_.

1. Glossy photographs or pages _____
2. Colored illustrations, paper or print _____
3. Photographs with dark background _____
4. Illustrations are poor copy _____
5. Pages with black marks, not original copy _____
6. Print shows through as there is text on both sides of page _____
7. Indistinct, broken or small print on several pages ✓
8. Print exceeds margin requirements _____
9. Tightly bound copy with print lost in spine _____
10. Computer printout pages with indistinct print _____
11. Page(s) _____ lacking when material received, and not available from school or author.
12. Page(s) _____ seem to be missing in numbering only as text follows.
13. Two pages numbered _____. Text follows.
14. Curling and wrinkled pages _____
15. Other _____

SOLAR MODULATION OF GALACTIC COSMIC RAYS: TECHNIQUES & APPLICATIONS

BY

JOHN S. PERKO
B.S., University of Detroit, 1973

A DISSERTATION

Submitted to the University of New Hampshire
in Partial Fulfillment of
the Requirements for the Degree of

Doctor of Philosophy

in

Physics

December, 1984

This dissertation has been examined and approved.

Lennard A. Fisk
Professor of Physics

Roger L. Arnoldy
Professor & Chairman, Physics
Director, Space Science Center

Harvey K. Shepard
Professor of Physics

Joseph V. Hollweg
Professor of Physics

Martin A. Lee
Associate Professor of Physics

3 Dec. 1984 JVH.
Date

TABLE OF CONTENTS

LIST OF ILLUSTRATIONS..... v

ABSTRACT..... vii

SECTION PAGE

INTRODUCTION..... 1

I. TIME-DEPENDENT MODULATION OF GALACTIC COSMIC RAYS..... 8

Introduction..... 8

Numerical Technique..... 10

An Illustrative Example..... 14

Concluding Remarks..... 22

II. COSMIC-RAY ELECTRON AND PROTON RECOVERY AFTER SOLAR MAXIMUM..... 23

Introduction..... 23

Technique..... 26

Results..... 28

Conclusions..... 31

III. SOLAR MODULATION OF GALACTIC ANTIPROTONS..... 32

Introduction..... 32

Assumptions..... 34

Force-field Approximation..... 36

Numerical Method..... 38

Results..... 39

Conclusion..... 46

IV. INFLUENCE OF A TERMINATION SHOCK ON ENERGY LOSS CALCULATIONS IN THE SOLAR WIND..... 47

Introduction..... 47

Technique..... 52

Results..... 58

Discussion..... 64

LIST OF REFERENCES..... 65

LIST OF ILLUSTRATIONS

INTRODUCTION.

Figure 1. Monthly average count from Mt. Washington neutron monitor..... 4

I. TIME-DEPENDENT MODULATION OF GALACTIC COSMIC RAYS.

Figure 1. Representative sample of solar wind disturbances... 17

Figure 2. Time profile of 1 GeV proton intensity at 1 and 20 AU with Pioneer 10 data superimposed..... 17

Figure 3. Time profile of 29 MeV proton intensity at 1 AU.... 19

Figure 4. Calculated hysteresis regression curve at 1 AU for 63 MeV and 10 GeV..... 19

Figure 5. Radial proton intensity gradient as seen by an imaginary spacecraft moving through the solar system..... 21

II. COSMIC-RAY ELECTRON AND PROTON RECOVERY AFTER SOLAR MAXIMUM.

Figure 1. Proton intensity at 1.5 GV versus electron intensity at 826 MeV over one solar cycle..... 29

Figure 2. Same as Figure 1 with protons at 5.0 GV..... 29

Figure 3. Cumulative proton intensity versus cumulative electron intensity from 747-909 MeV over same solar cycle as Figures 1 and 2..... 30

III. SOLAR MODULATION OF GALACTIC ANTIPROTONS.

Figure 1. Proton intensity spectra in interstellar space and at 1 AU: data compared to numerical calculations.. 40

Figure 2. Proton intensity spectra in interstellar space and at 1 AU: a numerical solution compared to the "force-field" approximation..... 40

Figure 3. Hypothetical interstellar spectrum of similar magnitude to "leaky-box" models with numerically modulated curve at 1 AU..... 42

Figure 4. Same as Figure 3 with interstellar spectrum multiplied by 9..... 42

Figure 5. Same as Figure 3 with interstellar spectrum multiplied by 90..... 44

Figure 6. Kinetic energy versus antiproton/proton ratios, combining the results from Figures 1 and 3..... 44

Figure 7. Same as Figure 6 with the antiproton interstellar spectrum multiplied by 30..... 45

Figure 8. Interstellar spectrum used by Tan & Ng [1983] with corresponding numerically modulated curve at 1 AU.. 45

IV. INFLUENCE OF A TERMINATION SHOCK ON ENERGY-LOSS CALCULATIONS IN THE SOLAR WIND

Figure 1. Monoenergetic interstellar spectrum at 50 MeV; resultant spectrum of accelerated particles at the termination shock boundary; modulated spectrum of particles at 1 AU..... 61

Figure 2. Monoenergetic interstellar injection spectra at 50, 200, 500 and 1000 MeV, and their resultant spectra at 1 AU..... 62

Figure 3. True interstellar proton spectrum along with resultant spectra at 1 AU for two cases: with a shock and without a shock..... 63

ABSTRACT

SOLAR MODULATION OF GALACTIC COSMIC RAYS: TECHNIQUES & APPLICATIONS

by

John S. Perko
University of New Hampshire, December, 1984

This thesis covers four topics in the theory of interplanetary cosmic-ray propagation:

The first part involves the time-dependent, spherically-symmetric, solar modulation of galactic cosmic rays. A numerical technique was introduced for the solution of this problem. A model for the solar-cycle variation in cosmic-ray intensity illustrated this method, using enhanced particle scattering regions. This model accounted for at least three key sets of observations: the cosmic-ray radial intensity gradients; the decrease in cosmic-ray intensity over the solar cycle; and the hysteresis between low and high-energy cosmic rays.

The second section contains an attempt to explain recent observations which show that cosmic-ray electrons are returning to higher intensities, characteristic of solar minimum, faster than cosmic-ray protons of about the same energy, the reverse of the previous eleven-year cycle. This section tests a suggested reason for the observations: velocity and rigidity differences between protons and electrons due to their different masses. The time-dependent, spherically-symmetric model of the first section generated the necessary

lag in the relative recovery rates, but only as observed in the previous solar cycle.

The third section involves the solar modulation of galactic antiprotons. It appears that a recent low-energy measurement of these particles has given cosmic-ray theorists trouble devising an interstellar spectrum to fit the observations. Using a steady-state, spherically-symmetric, numerical modulation code, a solution that reasonably fits the observed 1980 galactic proton spectrum at 1 AU implied that the modulation used for the data interpretation has been significantly underestimated.

The final section contains a spherically-symmetric, steady-state calculation of the effects of a strong termination shock in the heliosphere. In the end, high-energy particles cooling down in the upstream solar wind overwhelmed any accelerated low-energy particles, those which would be most affected by the shock. The overall effect of a shock on the near-Earth spectra seems negligible.

INTRODUCTION

In 1912, Victor Hess, through his balloon experiments, first demonstrated that the source of previously detected ionizing radiation was outside Earth's atmosphere. R. A. Millikan coined the phrase "cosmic rays." Today we know that Earth is bombarded by a variety of charged nuclei, mostly protons with a smattering of heavy elements, up to atomic number 60 or thereabouts. The question of origin is too complex to dwell on here, but most theories center on stars and supernovae for synthesis of the heavy elements, with supernovae, active galaxies and interstellar shocks supplying the acceleration. Whatever their origin, these particles represent the only direct sampling of the interstellar medium and of distant galactic objects such as supernovae and other exotics. This motivates the close study of these particles.

Most remarkable is the range of energies represented: from about 20 MeV up to 10^{21} eV and beyond. Below 20 MeV, particles are virtually excluded from the inner solar system by the Sun [Goldstein et. al., 1970] by a process that is the major subject of this dissertation (see below). Electrons, protons and other nuclei also seem to share an interstellar spectrum proportional to $E^{-2.6}$, where "E" is the total energy; a slight steepening has been observed at energies greater than 10^{15} eV [Longair, 1981]. The distribution of these particles in energy and space, however, suffers a complex rearrangement, or modulation, due to the Sun's pervasive influence in our galactic neighborhood. The instruments of the Sun's influence are the solar wind and the interplanetary magnetic field.

The solar wind is a continuous outflow of ionized gas, mostly protons and helium nuclei, accelerated somewhere at the base of the Sun's corona. (The corona itself is a cloud of similar gas surrounding the Sun, with a temperature of around 10^6 K.) The typical speed for this wind is around 400 km/s in the radial direction, though it ranges from about 300-800 km/s. The ram pressure of this flow holds back the interstellar medium to some 50-100 AU from the Sun [Holzer, 1979].

Attached to the surface of the Sun are the footpoints of the interplanetary magnetic field (IMF). The solar wind plasma is confined along these lines; that is, the lines are "frozen-in" to the plasma and the plasma and the field lines move together. In the steady solar wind the magnetic field lines are dragged out into interplanetary space, one line connecting all plasma emitted from the same point on the Sun. These lines occupy all of interplanetary space that we have probed. The simplest form of this field pattern, with the solar-wind speed constant, is an Archimedean spiral.

We consider here the superposition of small-scale fluctuations of magnetic intensity on this large-scale field. These fluctuations represent wave motions, turbulence and other disturbances which perturb the mean magnetic field. They scatter the cosmic rays in pitch angle, the angle between the velocity of the cosmic-ray particle and the mean magnetic field. It is this scattering which affects the distribution in space of cosmic rays below a few tens of GeV in energy. These scattering centers are also carried outward by the solar wind, thus helping to convect the cosmic rays outward when measured in the frame of the Sun. The lower the energy of the particle, the more difficult it is to make it upstream.

Evidence for this modulation goes well back in time. Forbush [1938] noticed sudden global decreases in cosmic-ray intensity and related them to geomagnetic disturbances. These decreases were measured at ground stations around the world. Since the early 1950's, ground-based monitors measuring energetic neutrons (representing cosmic rays of about 10 GeV) have been operating at several places. A data record from the neutron monitor atop Mt. Washington is shown in Figure 1 (Courtesy J. A. Lockwood). We see here an obvious periodicity correlated with the 11-year solar cycle: low cosmic-ray intensity at solar maximum and higher intensity at solar minimum. This modulation phenomenon has been subject to theoretical investigation for at least the last 25 years.

The first rigorous theory of modulation was described by Parker [1958], who envisioned a disordered magnetic field convected out by the solar wind. Coupled with this convection, the result of the wind's bulk motion, there is diffusion, the cosmic-ray scattering in phase space. These concepts were further detailed by Parker [1964] again, when he investigated the details of scattering at low and high energies and determined that the strongest scattering occurred when the magnetic irregularities were comparable in size to the cosmic particle's cyclotron radius.

Parker [1965, 1966] further refined the diffusion theory, calculating values for the diffusion coefficient, normally a tensor, which expresses phenomenologically the amount of scattering felt by the cosmic rays (see below). Jokipii [1966] calculated a diffusion coefficient from a statistical treatment of particle motion in a randomly fluctuating magnetic field. Gloeckler & Jokipii [1966] calculated a diffusion coefficient directly from a power spectrum of magnetic

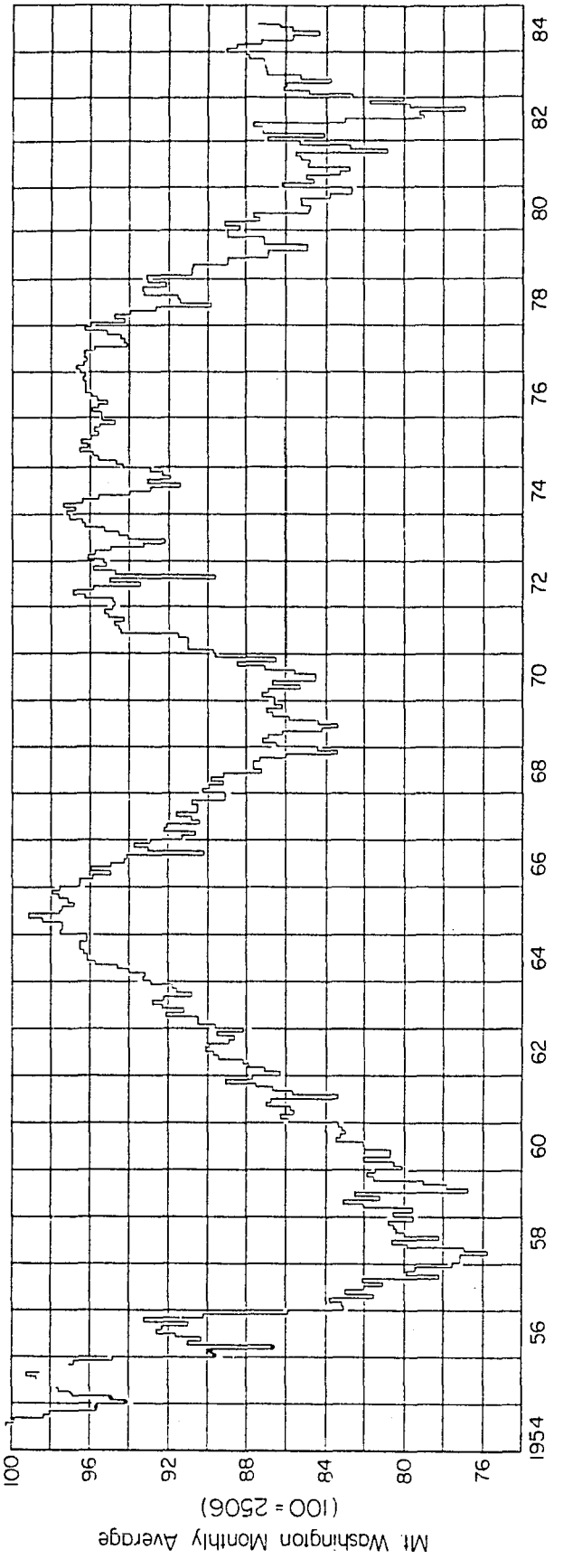

Figure 1. Monthly average (normalized) count from Mt. Washington neutron monitor. Neutrons represent cosmic rays of about 10 GeV (courtesy of J. A. Lockwood).

irregularities observed aboard spacecraft IMP I, II and III. Jokipii & Coleman [1968] did the same from Mariner 4 data. In general, diffusion along magnetic field lines is generally easier than diffusion across them. The generalization of the theory to this anisotropic diffusion was accomplished during this time [e.g., Parker, 1965; Jokipii & Parker, 1969].

Adding to the effects of convection and diffusion is adiabatic deceleration, the loss of cosmic-ray energy due to the expanding, spherical volume of the solar wind [Parker, 1965, 1966]. Convection, diffusion and adiabatic deceleration are combined in the master differential equation now used for cosmic-ray modulation, the Fokker-Planck equation (eqn. (1), Section I). Gleeson & Axford [1967] rederived this equation such that the energy loss term arises explicitly, rather than in an ad hoc manner.

At this juncture, it is clear that a range of solutions to the modulation problem are required to successfully interpret cosmic-ray data obtained from the inner solar system, since in situ sampling of interstellar material is not in the foreseeable future. Also, detailed knowledge of cosmic-ray modulation over different time scales and cycles is needed to understand historical records of cosmic-ray bombardment, such as tree rings containing C^{14}, a radioactive remnant of high-energy particle collisions in the atmosphere. The variation in the amount of this isotope over time can only be understood in the context of long-term solar modulation of the cosmic rays which are their source.

Analytic steady-state solutions to the convective-diffusive equation, without adiabatic deceleration, proceeded from Parker's [1958] original attempt, using an energy-independent diffusion coefficient and

spherical symmetry. Parker [1965] later extended his solutions to include adiabatic decelaration. Jokipii [1967] further added energy-dependence to the diffusion coefficient by using a form proportional to (Pv/c), where "P" is the rigidity of the particle (= pc/Ze), "v" is the particle velocity, "c" is the velocity of light, "p" is the particle momentum and "Ze" is the particle's charge. For particle energies greater than a few hundred MeV/nucleon, Gleeson & Axford [1968] found approximate solutions formally equivalent to those using a heliocentric "force-field" proportional to the particle's charge. Fisk & Axford [1969] extended these results down to a lower energy range (50-75 MeV/nucleon).

Full, numeric, steady-state solutions with spherical symmetry began with Fisk [1971a]. He obtained results that fit observed proton and helium spectra reasonably well over all energies, using realistic forms of the diffusion coefficient. Goldstein, Fisk & Ramaty [1970] used this technique to follow the Sun's effects on monoenergetic spectra. They found that particles with energies less than around 60-100 MeV/nucleon actually originate at higher energies, thus making it impossible to directly sample galactic cosmic rays at these energies. Indeed, protons less than about 20 MeV may be excluded altogether [see also Gleeson & Urch, 1971]. Fisk [1976] introduced solutions dependent on heliocentric latitude. His technique was modified for efficiency by Moraal & Gleeson [1975].

Approximate analytic time-dependent solutions with a time-varying diffusion coefficient were introduced by O'Gallagher [1975] and O'Gallagher & Maslyar [1976] to explain long-term variable observations related to the solar cycle. These effects are detailed further on.

Hatton [1980] used the data from large solar flares to model the solar cycle with fair results. A full numeric, time-dependent, spherically-symmetric solution with a reasonably realistic model of the Sun's 11-year cycle was finally realized by Perko & Fisk [1983], the subject of the next section.

Subsequent sections deal with full numeric solutions both time-dependent and time-independent. These are used to contribute to the solution of three current astrophysical problems of interest: The first is the question of relative recovery rates of electrons and protons during the decline from solar maximum and how solar cycles differ in their effects. The second section straightens out some confusion over the use of solar modulation in the analysis of recent cosmic-ray balloon data. The final section deals with the effects of an alleged standing shock at the boundary of the heliosphere: Since a strong shock should accelerate particles, how does this affect cosmic-ray distributions in the inner solar system?

I. TIME-DEPENDENT MODULATION OF GALACTIC COSMIC RAYS

Introduction

To date, models for the solar modulation of galactic cosmic rays have been confined to steady-state [e.g., Parker, 1965; Gleeson & Axford, 1967; Fisk, 1971a, 1976, 1979]. The feeling was that changes occur slowly enough in the heliosphere to allow this. The development of these solutions assumed that the modulating region of the Sun was only several AU in radius. The solar wind travels this distance in only about ten days. In this case, an equilibrium could occur, and the region could be assumed free of such disturbances as flare-generated shocks for long periods, resulting in a steady state. We now know that Pioneer 10, the most distant spacecraft ever in contact with Earth, has yet to cross the heliospheric boundary. It is, at this writing, over 30 AU from the Sun. The boundary then is at least this far, though more likely 50-100 AU [Webber & Lockwood, 1981]. Since the transit time of the solar wind over this distance is about a year, conditions in different parts of this cavity can vary markedly, especially during the most active periods in the Sun's cycle, during which solar conditions change rapidly. Shock disturbances passing through on their way to the outer heliosphere can also produce effects on the cosmic rays that persist long after the shock's passage [McDonald et. al., 1981a].

A striking observational effect of obvious time-dependence is the so-called hysteresis effect. As the Sun approaches its maximum activity in the 11-year cycle, the cosmic rays decrease in intensity.

However, as the Sun recovers from this maximum toward its quiet time, the recovery of the lower-energy particle intensities lag behind the recovery of the higher-energy intensities (see Figure 4); i.e., the lower-energy particles recover more slowly from their bout with high solar activity. O'Gallagher [1975] and O'Gallagher & Maslyar [1976] first introduced approximate solutions for modulation equations, which attribute this hysteresis to time-dependent effects.

The model from which I proceed is spherically-symmetric, so transport of cosmic rays in heliographic latitude is considered unimportant. The reason is twofold: First, this first time-dependent numerical model makes heavy demands on computer time and storage. The inclusion of latitude effects would overburden all but the most powerful computers. Second, exclusion of latitude transport is supported by recent observations. For example, McDonald et. al. [1981a,b] reported that disturbances in the solar wind, presumably generated by shock waves from solar flares, propagate radially outward and successively depress the cosmic-ray intensity at Earth and Pioneer 10, keeping it depressed for a long time. If transport in latitude were important, we would see particles filling in from the sunward side. The observers did not see this.

To illustrate the central numerical technique, I introduced a simplified model of the solar cycle, which accounted for the observed variation in cosmic-ray intensities, the observed spatial gradients, and provided a natural explanation for the hysteresis effect.

The results of this Section were first published by Perko & Fisk [1983].

Numerical Technique

Consider a time-dependent, spherically-symmetric model, in which the cosmic-ray omni-directional distribution function "f" is the number of particles per unit volume of phase space ($d^3r\ d^3p$) averaged over particle direction. The behavior of this function can be described by [Parker, 1965; Gleeson & Axford, 1967; Fisk et. al., 1973]

$$\frac{\partial f}{\partial t} = \frac{1}{r^2}\frac{\partial}{\partial r}\left(r^2\ \kappa\ \frac{\partial f}{\partial r}\right) - V\frac{\partial f}{\partial r} + \frac{1}{r^2}\frac{\partial}{\partial r}\left(r^2 V\right)\frac{p}{3}\frac{\partial f}{\partial p} \qquad (1);$$

where "f" is related to the particle differential intensity "j" by $j = p^2 f$; j is the value most often reported by observationalists. Also, "t" is the time, "r" is the heliocentric radial distance, "V" the solar-wind speed, "p" the particle momentum, and "κ" the diffusion coefficient for radial propagation. I assumed that particles move only along magnetic field lines. According to Parker [1967], κ is related to $\kappa_{\parallel}$, the diffusion coefficient for propagation along field lines, by $\kappa = \kappa_{\parallel}\cos^2\Psi$, where "$\Psi$" is the angle between the field lines and the heliocentric radial direction. Although this angle varies a great deal with radius, it is an observed fact that the diffusion coefficient does not depend on radius, since the radial gradients are known to be very small. Therefore, for my purposes, I can make κ a constant in radius and not dependent on Ψ. The first term on the right side of equation (1) describes the effect of diffusion; the second and third terms comprise the effects of convection and adiabatic deceleration in the expanding solar wind. This equation cannot be solved analytically without simplifying assumptions which are unrealistic in the solar wind. Therefore, let us turn to a numerical solution.

I applied the Crank-Nicholson finite-difference technique to solve (1), a parabolic, partial differential equation [Diaz, 1958]. The derivatives in (1) are replaced by central-difference formulae which relate values of "f" at r, r-Δr and r+Δr; t and t+Δt; and p and p-Δp. Respectively, Δp, Δr and Δt are the momentum, radius and time intervals used in the computation.

For convenience, equation (1) was rewritten in terms of ln(p) and stepped in equal intervals of ln(p). The momentum steps will then be large at high momenta where the modulation is small, and small at low momenta where the modulation is large.

I assumed that particles with high momentum are essentially unmodulated. Thus I let $f(p=p_o)$ be constant in radius and time and be equal to the unmodulated interstellar spectrum at p_o. For most applications, p_o equivalent to an energy of 60 GeV/nucleon is sufficiently high. This is one boundary condition. Incidentally, Moraal & Gleeson [1975] use a "force-field" solution at the high end of momentum, which allows them to drop this upper limit considerably and save computer time.

At the outer boundary, r=R, I took "f" equal to the unmodulated interstellar spectrum with the assumed form

$$f \propto (T_o^2 + p^2c^2)^{-1.8} / pc \qquad (2),$$

where "T_o" is the particle rest energy and "c" is the speed of light. This form corresponds to a differential number density spectrum which is a power law in total energy, with a spectral index of 2.6. This form has been commonly assumed in modulation studies [e.g., Fisk, 1971a, 1976].

For the boundary condition at r=0, I assumed that the differential streaming, or current density "S" is zero at all times, or equivalently [Fisk et. al., 1973]

$$-\frac{V}{3} p \frac{\partial f}{\partial p} - \kappa \frac{\partial f}{\partial r} = 0 \qquad (3)$$

This choice prohibits spurious particles from entering the modulation region at r=0.

The first time step was just the steady-state numeric solution generated by Fisk [1971a]. Values for "f" at all radial steps are assumed at highest momentum "p_o." The finite-difference form of equation (1) (with $\partial f/\partial t=0$) determines the values of "f" for all radial steps at each lower momentum step. At each of these momentum steps, a set of linear equations from the central-difference formulae must be solved to yield "f" at all radii. These equations form a simplified tri-diagonal matrix which eases the calculation. The solution is subject to the boundary conditions at r=0 and at the edge of the modulation region (r=R).

The solution for subsequent time steps was straightforward. The solution at time "t" was known. The initial solution at $p=p_o$ was again assumed. Then the full finite-difference equation for (1), including the "t" derivative, determined the solution at $t+\Delta t$ and $p_o-\Delta p$ for all radial steps, again subject to boundary conditions at r=0 and r=R. This procedure was followed for each lower momentum step at the same $t+\Delta t$ until the lowest chosen momentum was reached. The solution at that time step was then complete.

Solutions using Crank-Nicholson techniques are typically stable, at least in textbooks. For reasonable choices of κ and V, this should hold. However, I found that solutions tended to drift slowly in

time away from equilibrium values, unless the time-step size chosen was sufficiently small. It appears that the step size must be less than the transit time of the solar wind over the radial step. For my solutions, $\Delta t = 0.5\ \Delta r/V$ seemed to work.

An Illustrative Example

I assumed, as suggested by the Pioneer 10 and 11 data, that the solar-cycle variation of the cosmic-ray flux results from changes in the number of shock-generated disturbances in the solar wind [McDonald et. al., 1981a,b]. Let this be a basis for a solar-cycle modulation model.

I assumed as well that cosmic rays move only along magnetic field lines, that the radial diffusion coefficient is constant in time in the undisturbed solar wind, and that it is given by

$$\kappa = 4.3\ \beta\ (2 + P^2)\ 10^{21}\ cm^2/s \qquad (4),$$

where "β" is the ratio of particle speed to the speed of light and "P" is particle rigidity in units of GV. This form is consistent with solar-flare particle studies at low energies [e.g., Zwickl & Webber, 1977], with the predictions of quasi-linear theory at high energies [e.g., Jokipii, 1971], and with observations of proton and helium spectra in undisturbed conditions. The magnitude of κ has been chosen to yield the observed radial gradient of about 2-3%/AU for protons $\gtrsim$ 60 MeV [McKibben et. al., 1975; McDonald et. al., 1981a].

Regions of enhanced scattering, where the diffusion coefficient decreases, can be superposed on the undisturbed solar wind. These may occur in the wake of a large flare-generated shock, or perhaps when a series of shocks creates a disturbed region. For simplicity I allowed the diffusion coefficient in (4) to vary in each disturbed region as $[1 - \alpha \sin^2(\pi r/L)]$, where $\alpha = 0.9$ and "L", the width of the disturbance, was 2 AU; the maximum decrease of κ was 90% of the undisturbed value. The value of "L" was chosen as roughly comparable to the size of compression regions measured by Pioneer and Voyager spacecraft [see, e.g.,

Burlaga, 1983; McDonald et. al., 1981b]. The size of α was adjusted to give a proton intensity decrease at solar maximum that matched the observations.

Shocks in the solar wind at Earth and beyond do not propagate appreciably faster than the solar wind itself, i.e., by a $\lesssim$ 100 km/s difference [e.g., Hundhausen, 1972]. Furthermore, disturbed regions generated by shocks may outlive the shocks themselves [Burlaga et. al., 1983]. So to simplify, I assumed that the disturbed regions caused by these shocks were convected outward at the solar wind speed "V," which I further assumed was constant over the solar cycle and equal to 400 km/s.

A constant solar-wind speed causes the magnetic field lines to execute an Archimedean spiral, on the average. Further, I assumed that cosmic rays move only along these lines. Under these circumstances, equation (1) can describe the behavior of "f" on a single magnetic flux tube, as discussed in detail by Ng [1972]. Consequently, the disturbed regions in the model need not be large, but only threaded by the field lines of the flux tube.

I assumed that the number of disturbed regions in the solar wind varied smoothly over the solar cycle, from one passing Earth every 4 months at solar minimum to one passing every 2 weeks at solar maximum. This frequency of occurrence was chosen to fit the rate of proton intensity decrease seen by spacecraft (see Figure 2). The time profile of the passage of disturbed regions seen at Earth was assumed to be symmetric about a time at solar maximum, i.e., the profile of disturbed regions in the first half of the solar cycle, before solar maximum, was the mirror image of the profile in the second half. Figure 1 shows a snapshot of the disturbances in the solar system from 0-100 AU at a time

near solar maximum. The vertical scale is the percent decrease in the diffusion coefficient from its undisturbed value in equation (4).

The initial condition of the model solar system is that of complete quiet, with no disturbances present. At the end of the calculation, the system is again free of disturbances and allowed to relax to as close to the initial state as possible.

I set the outer boundary of the modulation region at r = R = 100 AU, and generated a numerical solution to (1) over a period of 4,000 days (about 11 years), from one solar minimum to the next, using the above assumptions. The resulting time profile for the 1 GeV proton intensity behavior at r = 1 and 20 AU is shown in Figure 2.

Superposed on the 20 AU curve in Figure 2 are 5-day running averages of the intensity of protons $\gtrsim$ 60 MeV (a mean energy of around 1 GeV), as recorded by Pioneer 10 (courtesy of W. R. Webber). I neither expected nor attempted a detailed fit between theory and observation. The computed results were valid for a single flux tube at a fixed radius (r = 20 AU); Pioneer 10, of course, observes many flux tubes during this period over a range of radial distances on either side of 20 AU. Nonetheless, the calculation yielded a rate of intensity decrease between solar minimum and maximum that reasonably agreed with the observations.

The inset in Figure 2 shows an enlarged version of the intensity decreases that resulted when the disturbed regions reached r = 1 and 20 AU in succession. The dotted lines connect intensity decreases produced by the same disturbance, i.e., after passing 1 AU the disturbance was convected outward at 400 km/s and crosses 20 AU about 75 days later.

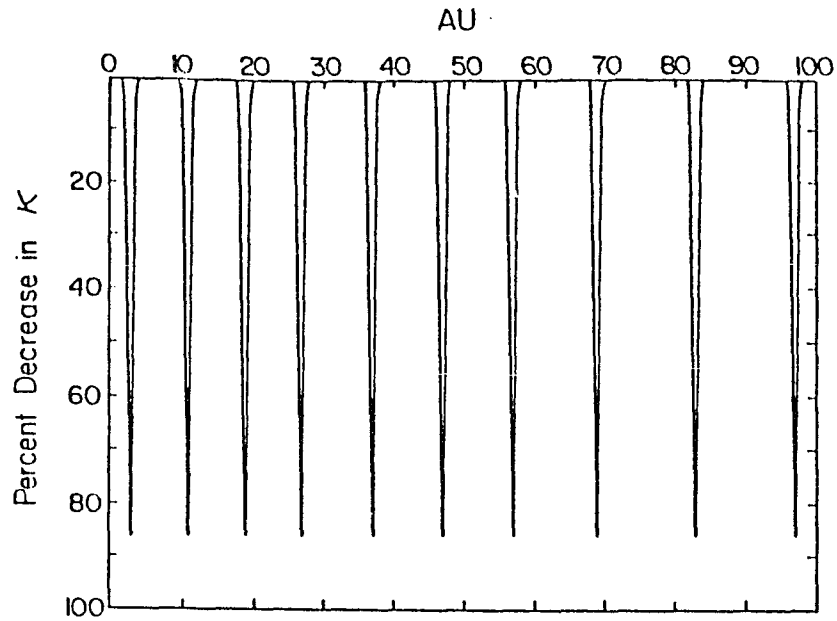

Figure 1. Representative sample of solar wind disturbances used for the model in this section. Vertical axis is the percent decrease in the diffusion coefficient from the quiet-time value in an undisturbed solar wind. This shows a group of disturbances at a time approaching solar maximum.

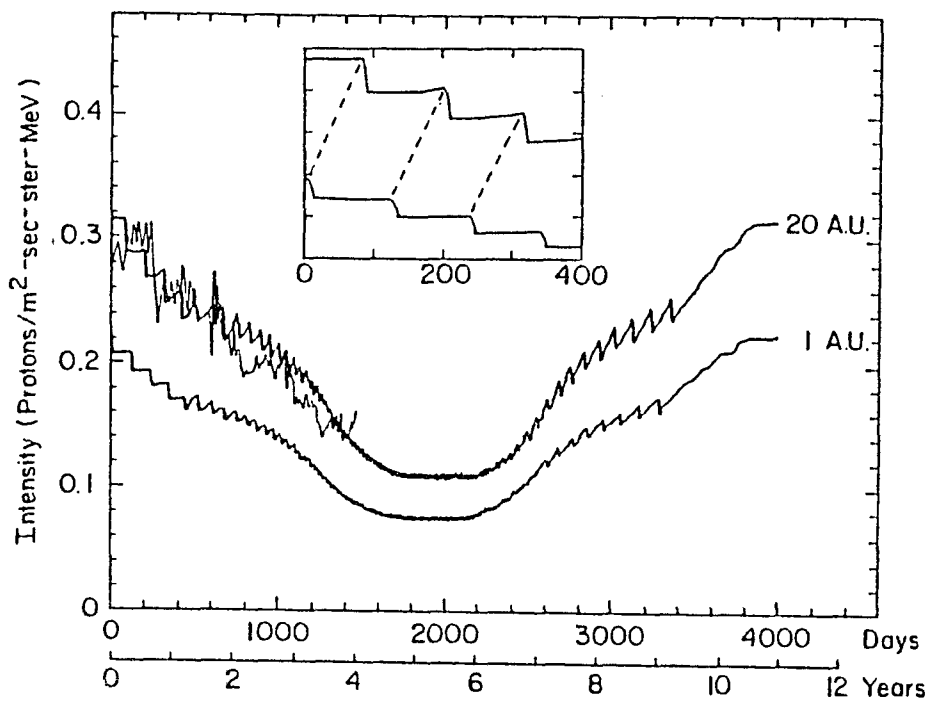

Figure 2. Calculated time profile of 1 GeV proton intensity at 1 AU and 20 AU over the simulated solar cycle. Superimposed on the 20 AU line is Pioneer 10 measurements of cosmic-ray proton intensity (courtesy of W. R. Webber); data spans Sept., 1977, to May, 1981.

Figure 3 is the calculated time profile of the 29 MeV proton intensity at 1 AU. The decrease in intensity in the figure is a factor of 9, which agrees fairly well with the observed solar-cycle variation.

In the model presented here, a disturbed region partially restricted the inward movement of cosmic rays until that region passed out of the modulation cavity at R = 100 AU. Then the cosmic rays could propagate in more freely. Since higher-energy particles are more mobile in the solar wind (cf. equation (4), where κ is largely proportional to the mean free path of the particle), they will do this more readily than lower-energy ones. A close examination of Figures 2 and 3 reveals this. Following solar maximum, the number of disturbed regions began to decrease, and the 1 GeV proton intensity started recovering before that of the 29 MeV protons.

Figure 4 illustrates this hysteresis effect more clearly. I have plotted a regression curve of the 10 GeV proton intensity versus the 63 MeV proton intensity, calculated over the solar cycle. These energies were chosen to match those typical of regression plots of neutron monitor versus low-energy satellite data. In fact, the curve in Figure 4 was smoothed with a 27-day average, the usual interval for this data. Clearly, the hysteresis resulted in a low-energy proton intensity about two times higher in the declining phase than in the recovering phase. This agreed fairly well with the observed hysteresis effect at these energies [e.g., Van Hollebeke et. al., 1972].

Hysteresis can also be measured in terms of a time lag. Notice in Figure 4 that the 10 GeV proton intensity returned to its initial value (in the undisturbed wind) before that of the 63 MeV

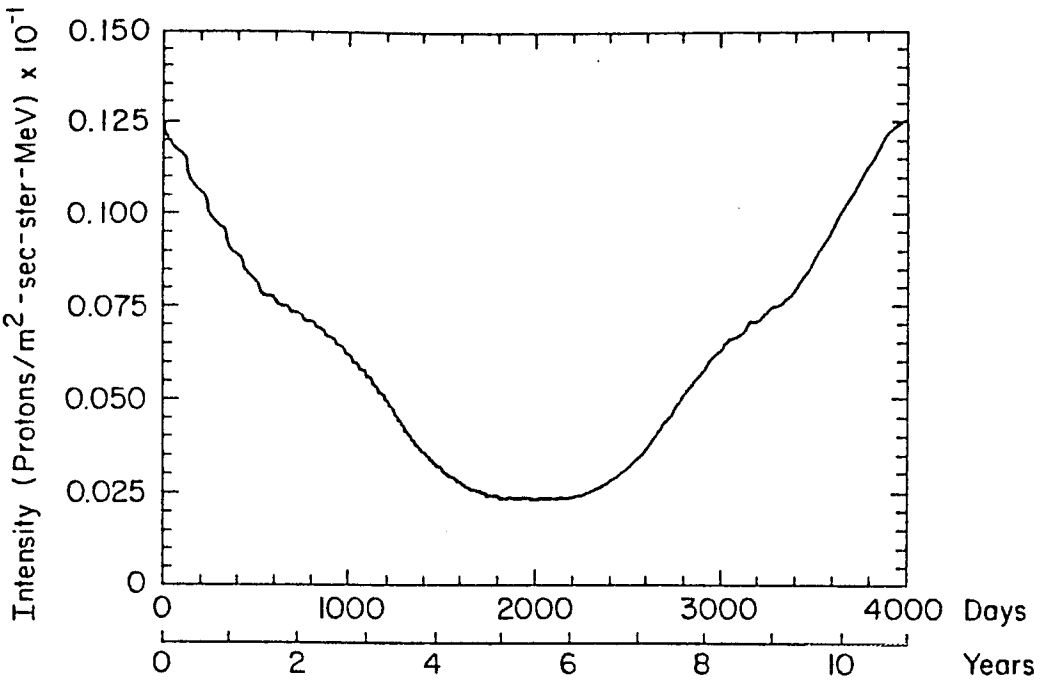

Figure 3. Calculated time profile of 29 MeV proton intensity at 1 AU over the simulated solar cycle.

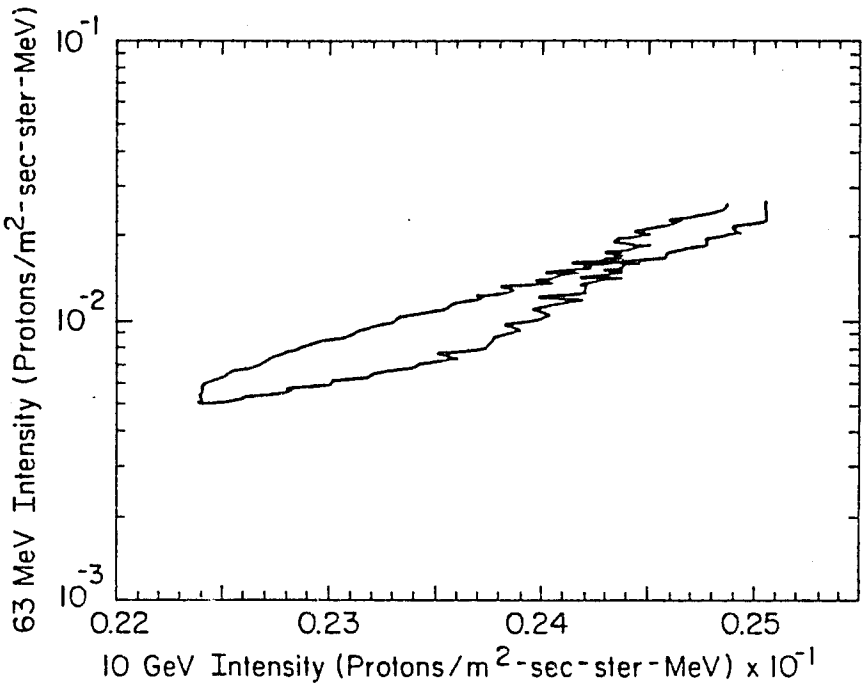

Figure 4. Calculated hysteresis regression curve with 27-day averaging: 63 MeV vs. 10 GeV proton intensity over the solar cycle. (Upper line of the curve is the declining phase of the cycle; lower line is the recovering phase.

protons. The high-energy protons returned to their initial quiet-time state about 260 days before the low-energy protons, as measured by the calculated results. The hysteresis effect plotted in Figure 4 depended principally on the size of the modulation region (100 AU in my example) and was not particularly sensitive to other parameters in the model, so long as they were chosen to satisfy observed constraints.

The choice of diffusion coefficient in equation (4) ensured that the calculated radial gradient of the 1 GeV proton intensity (or equivalently the integral proton intensity of energies $\gtrsim$ 60 MeV) was the observed value of 2-3%/AU in the undisturbed solar wind. We need to verify that the calculated gradient in the presence of the disturbed regions, with their large diffusive fluctuations, also agreed with observations. In doing this, I noted that spacecraft measurements of the gradient are formed by looking for average trends while comparing the intensity observed by an outwardly moving space probe and a reference spacecraft at Earth.

Figure 5 is the calculated ratio of the 1 GeV proton intensity at $r = r_s$ to the corresponding intensity at 1 AU; r_s is the radius in AU of an imaginary spacecraft moving radially outward at 3 AU/year, about the speed of Pioneer 10. The two smooth curves in the figure are the function $\exp[G(r_s-1)]$, with "G", or the equivalent average gradient, set at 2%/AU and 3%/AU. This graph closely resembles the graph of Pioneer 10 integral gradient measurements drawn by Bastian et. al. [1981]. Again, I caution that this result was calculated on a single flux tube.

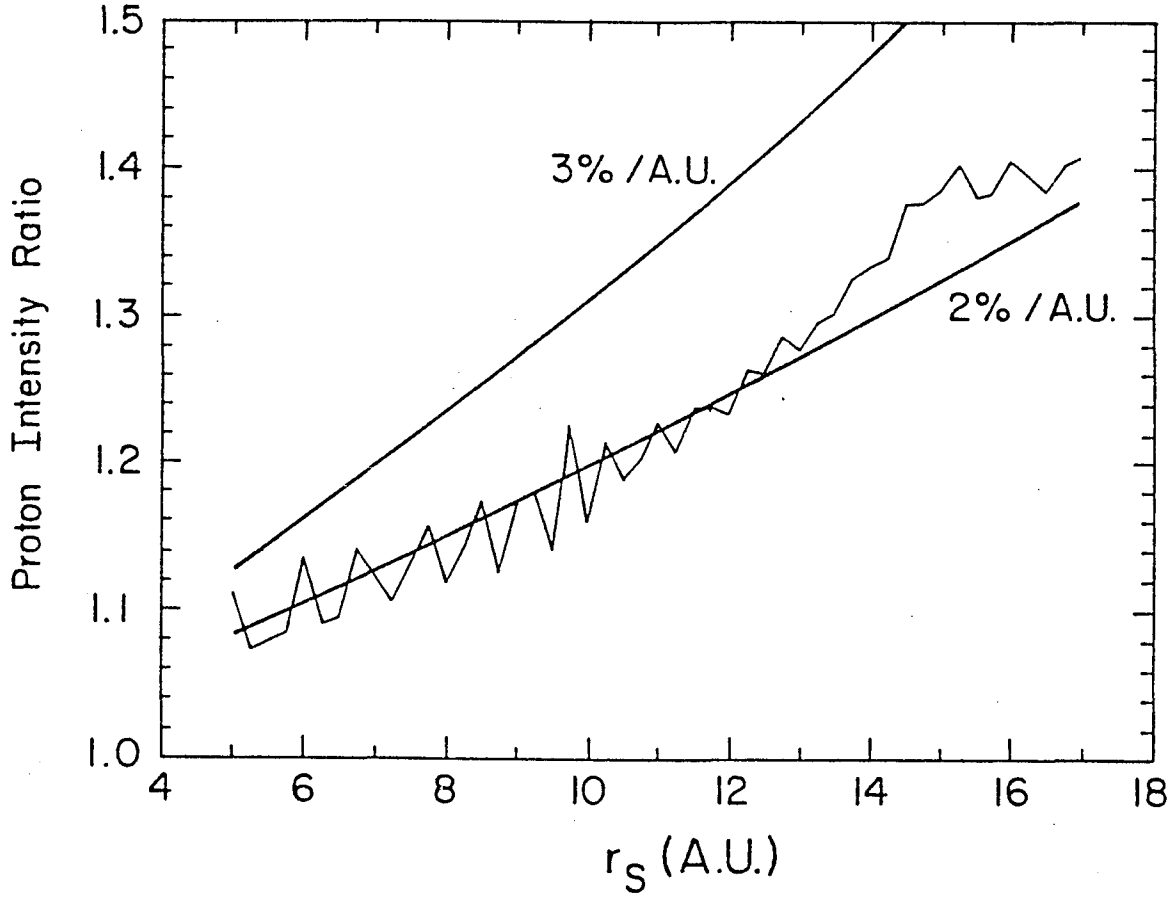

Figure 5. The ratio of the intensity of 1 GeV protons at r_s to the intensity at 1 AU vs. r_s, the distance of an imaginary spacecraft from the Sun. The smooth lower curve is a plot of the function $\exp[G(r_s-1)]$, where G = 2%/AU; the smooth upper curve is the same function with G = 3%/AU.

Concluding Remarks

I have introduced a numerical technique for solving the time-dependent equation for the modulation of galactic cosmic rays, ignoring transport in heliographic latitude. To illustrate this technique, I have described a simplified model of the solar-cycle variation in cosmic-ray intensity; this variation is caused by changes in the number of enhanced scattering regions in the solar wind. The model yielded the observed solar-cycle changes in the intensity at different energies and the observed spatial gradient. It provided as well a natural explanation for the cosmic-ray hysteresis effect. These results indicate the necessity of explicit time-dependence in the solution of cosmic-ray transport over the solar cycle.

The hysteresis effect shown in Figure 4 was a measure of the importance of time-dependent effects in the modulation process. In this model, the time profile of the total number of disturbances in the solar wind was symmetric about solar maximum. That is, the frequency with which these disturbances pass a fixed point in space rose at some specified rate and reached a peak frequency at solar maximum. After solar maximum, this frequency declined at the same rate, creating a mirror image of the first half of the cycle. So when I ran a modulation solution with a series of independent steady states, calculated at different times during the cycle, the behavior of the particle intensity during recovery was the reverse of the behavior during decline, with no hysteresis. However, as seen in Figure 4, time-dependent effects resulted resulted in a difference of about two in the intensity of lower-energy particles between the decline and recovery phases.

II. COSMIC-RAY ELECTRON AND PROTON RECOVERY AFTER SOLAR MAXIMUM

Introduction

The comparative study of galactic cosmic-ray protons versus electrons has a direct bearing on whether, among other things, gradient and curvature drifts in a highly-ordered interplanetary magnetic field (IMF) have a significant effect on solar modulation of galactic cosmic rays [see, e.g., Jokipii et. al., 1977; Jokipii & Levy, 1977; Lee & Fisk, 1981]. The opposite charges of the proton and electron are the key. If indeed drifts are important, charge-dependent effects will begin to show in the data. Let me crudely illustrate.

From first-order orbit theory [Isenberg & Jokipii, 1979],

$$\langle V_D \rangle = \frac{pvc}{3ZeB^4} [B^2(\nabla \times \underline{B}) + \underline{B} \times \nabla B^2]. \qquad (1)$$

where "V_D" is the drift velocity of the particles in the magnetic field "$\underline{B}$," with charge "Ze," momentum "p" and velocity "v," averaged over all pitch angles. This form assumes that the particles' gyroradii are much smaller than any scale of inhomogeneity of the magnetic field and that there is an isotropic pitch-angle distribution. The derivation of this equation also implies that the particles considered must be of relatively low rigidity. Nonetheless, the dependence of drift direction both on the sign of the charge and the direction of the average magnetic field is clear from this simplified expression. Theoretical calculations by Jokipii and his collaborators have resulted in average drift speeds at or exceeding the solar wind plasma speed.

Recently published analyses of galactic cosmic-ray data gathered over the last solar cycle (1977-1983), especially for electrons, indicate discrepancies between modulation theory and observation by the dissimilar behavior of cosmic rays over the last two solar cycles. Evenson et. al. [1983] report good agreement between proton/helium ratios observed from 1965-1969 and steady-state modulation theory, but poor agreement for theory versus proton/electron and helium/electron ratios. Another analysis by Evenson & Meyer [1984] shows that since the last solar maximum in 1981, electrons of about 1 GeV are recovering more rapidly than protons of about the same energy (though different rigidity). This behavior, a "hysteresis" (see Section I), is opposite to that of the previous solar cycle, as reported by Burger & Swanenburg [1973]. In that epoch, the protons recovered faster.

One possible (known) cause is the difference in rigidity and speed between the electrons and the protons. Evenson & Meyer [1984] compared protons between 1.5 and 5.0 GV (0.83 and 4.15 GeV) and electrons at 828 MV (828 MeV). Since the diffusion coefficient, used to model the particle scattering in the heliosphere, is some function of particle rigidity, this difference could show up in the cosmic-ray distribution using a time-dependent calculation over a solar cycle. The diffusion coefficient also depends on β, the speed of a particle divided by the speed of light. For electrons anywhere near 828 MeV, β is practically one, while for the protons considered here it ranges from about 0.85 to 0.99. This is due to the large difference in mass between protons and electrons. In this section, I will test whether these differences affect the hysteresis through the diffusion coefficient.

It appears that for reasonable values of the diffusion coefficient, a slight hysteresis resulted for the energies in question. However, the hysteresis went in the sense of the Burger & Swanenburg data; that is, the protons recovered more rapidly than the electrons, whereas for the the more recent solar cycle, the electrons have had a quicker recovery.

Technique

The technique used to calculate the modulation for this Section was the much the same as in Section I [see also, Perko & Fisk, 1983], with a few differences. It is the spherically-symmetric, time-dependent, cosmic-ray transport model which solves equation (1), Section I. One calculation was done for protons, one for electrons. The boundary conditions were similar: The differential streaming was set to zero at r = 0 to preclude a source of spurious particles at the origin, as in Section I. The boundary at the outer edge of the modulation region, at r = 100 AU, consisted of an interstellar spectrum of protons or electrons. The proton spectrum was a power law in total energy with a spectral index of -2.6, again as before [see, e.g., Fisk, 1971a, 1976]. The electron spectrum was calculated directly from radio observations of synchrotron radiation and reported by Cummings *et. al.* [1973]:

$$j(m^2 \text{ sec sr GeV})^{-1} = 121.416\ E^{-1.8} \qquad \text{for } E < 2 \text{ GeV}$$

$$= 197.241\ E^{-2.5} \qquad \text{for } E > 2 \text{ GeV}$$

where "E" is the total energy of the electron in units of GeV.

The quiet-time diffusion coefficient took the following form:

$$\kappa(cm^2/sec) = 2.274 \times 10^{22}\ \beta \qquad \text{for} \quad P < 2 \text{ GV}$$

$$= 1.137 \times 10^{22}\ \beta\ P \qquad \text{for} \quad P > 2 \text{ GV}$$

where "P" is particle rigidity in GV. This form was chosen to give the most mobility to the electrons, while remaining physically plausible, particularly at low energies [Zwickl & Webber, 1977]. Specifically, the cutoff rigidity at 2 GV was probably as large as it could be; the higher it is, the more the diffusion coefficient depends only on β. The larger β for electrons, noted above, gave the electrons recovering from solar

maximum a larger diffusion coefficient than the protons, thus more mobility for them. If this does not help the electrons recover more quickly, other explanations for the current observations will likely be needed.

The same crude model of the solar cycle used in Section I was used here. To simulate large, flare-related disturbances in the solar wind, small regions(2 AU-wide) where the diffusion coefficient κ drops dramatically were sent out from the origin, causing decreases in the cosmic-ray intensity as they went by. They travelled at the solar wind speed. These disturbances, where κ dipped by as much 90%, came in increasing frequency, representing the Sun in its period of rising activity; they came less frequently as the Sun's activity would decrease. Thus an entire solar cycle was covered, from one minimum to the next.

Results

The results of this numerical integration are shown starting in Figure 1. It is a regression plot with the electron intensity at 826 MeV on the vertical axis and the 1.5 GV proton intensity on the horizontal; Figure 2 is the same with protons at 5 GV. Figure 3 plots the combined proton intensity between 1.5 and 5 GV against the combined electron intensity from 747 to 909 MeV, the approximate energies plotted by Evenson & Meyer [1984]. The points plotted were 27-day averages connected in time from start(S) to finish(F). A noticeable hysteresis is present in the last two, although the electrons were lagging here, as they do in Burger & Swanenburg [1973]. In Evenson & Meyer [1984], it is the protons which lag behind the electrons.

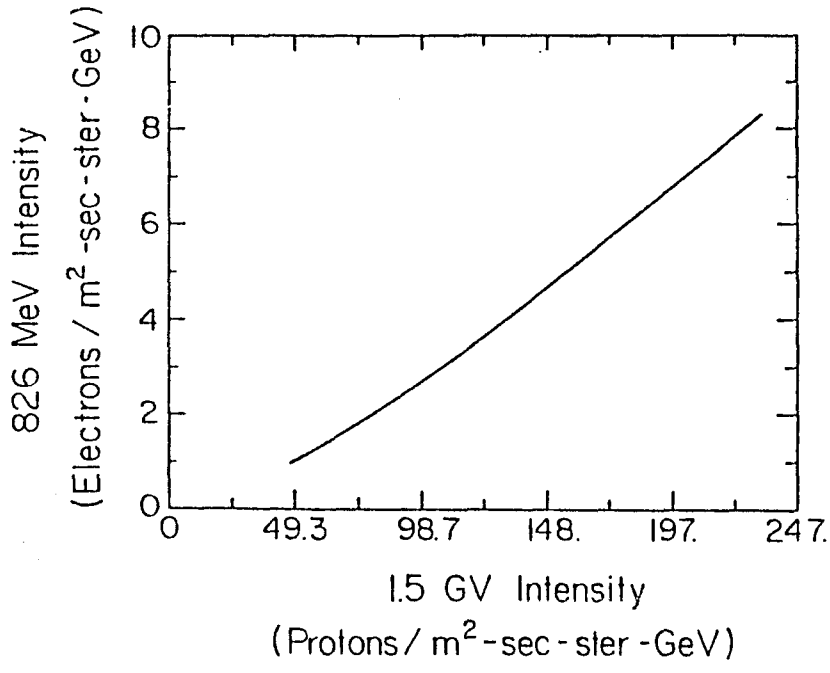

Figure 1. Proton intensity at 1.5 GV versus electron intensity at 826 MeV over one full solar cycle; points traced out are 27-day averages.

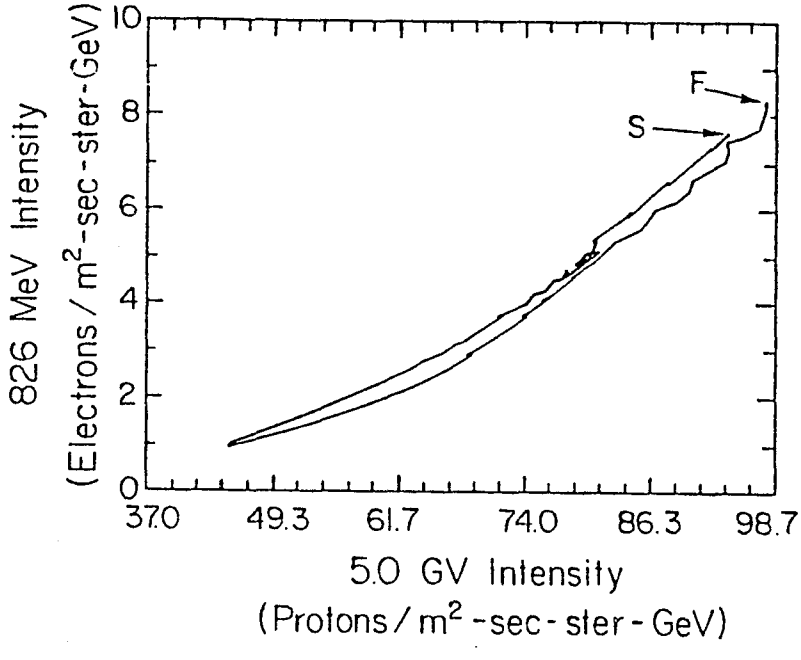

Figure 2. Same as Figure 1 except with protons at 5.0 GV from one solar minimum (S) to the next (F).

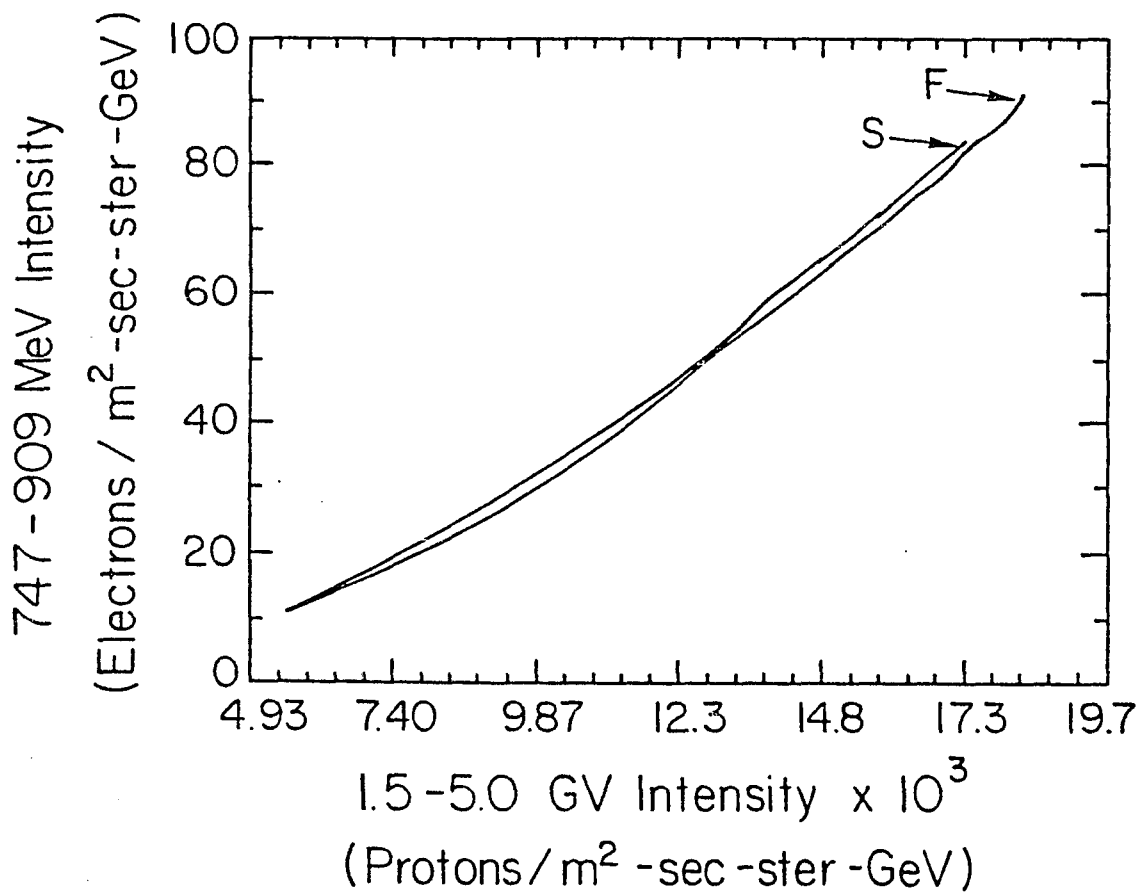

Figure 3. Cumulative proton intensity from 1.5-5.0 GV versus cumulative electron intensity from 747-909 MeV over same cycle as Figures 1 and 2; these energies are approximately those measured by Evenson & Meyer [1984].

Conclusions

The results from Section I have been extended here to include numerical electron modulation solutions over a solar cycle. The behavior of electrons and protons of about 1 GeV was compared over this cycle; the calculated proton intensity recovered more quickly in the inner solar system than the calculated electron intensity. This was true even under conditions strongly favoring a more mobile electron population.

The fundamental observational fact to explain is the reversal of the hysteresis over the two contiguous solar cycles: Protons recovered faster than electrons during the Sun's decline to minimum activity in the late 1960's, while electrons are recovering faster during the current decline. The reasons for this are still unclear.

Drifts combined with the polarity reversals that took place during the previous cycle have been cited as a possible cause [Evenson & Meyer, 1984]. The evidence against drifts cited in Section I applies only to protons. There, McDonald et. al. [1981a] saw sudden, strong cosmic-ray intensity drops that stayed at a low level for a long time; they saw no protons filling in from the sunward side.

The other possible cause involves the role of cross-field diffusion on species other than protons. Fisk [1976] has shown that extremely small variations in the latitudinal diffusion coefficient can alter the intensity near Earth by factors of five or so. How electrons and protons fare together in these two-dimensional, time-dependent models has yet to be calculated.

III. SOLAR MODULATION OF GALACTIC ANTIPROTONS

Introduction

Various researchers have conducted balloon flights to measure cosmic antiprotons (p^-), those p^-'s which are presumed to originate outside the heliosphere. In 1979, Golden et. al. [1984] measured antiproton-proton (p^-/p^+) ratios in the interval between 4.4 and 13.4 GeV. Bogomolov et. al. [1979] reported a ratio in the range of 2-5 GeV. Most recently, Buffington et. al. [1981] made measurements down to 200 MeV.

Golden et. al.'s data and that of Bogomolov et. al. have stirred much interest among cosmic-ray theorists, but it is Buffington et. al.'s low-energy datum that has confounded attempts to calculate a plausible interstellar p^- spectrum. They find a flux of antiprotons at 200 MeV over two orders of magnitude greater than expected.

Since all of these data are "top-of-the-atmosphere," that is, corrected to a flux in near-Earth space from balloon flights in the upper atmosphere, solar modulation must be taken into account when trying to infer an interstellar spectrum. At 1 AU, the p^- particles have traversed over 98% of the heliosphere, the region over which solar modulation is felt by the particles. We would expect considerable changes in the spectrum after such a journey.

It is not my intent here to specifically take issue with any of the above measurements, although there are others who may wish to do so. Instead I wish to focus on the way modulation is used to derive the interstellar spectra, or, in other words, to "demodulate" the data.

It appears as if workers in this field are seriously underestimating the magnitude of this modulation and in some cases ignoring it altogether. Furthermore, when the modulation is done correctly, we will see that an unreasonably steep slope would be necessary on the high-energy side of the galactic spectrum to fit both the low-energy and high-energy data at 1 AU. Let us start by detailing two reasonable assumptions used in many applications of modulation theory and that apply here.

These results were first presented by the author at the General Meeting of the American Physical Society, April 23-26, 1984 [Perko et. al., 1984].

Assumptions

First, I assumed time-independence, a "steady-state" solution. All of the p^- data considered here were taken right at solar maximum (1979-80). Since this is within a two-year period at solar maximum, fluxes at 1 AU were changing sufficiently slowly, allowing a time-independent solution. One way to see this is in Figure 3, Section I. This is a plot of the intensity of 29 MeV protons versus time as calculated by the numerical model of Section I. The variation of intensity within two years either side of solar maximum was less than a factor of 5/2, which was small compared to the discrepancies in modulation predictions, as we will see later. In addition, note in Figure 1 of Section I that the Mt. Washington monthly neutron monitor average (representing cosmic rays of about 1 GeV) varies by only about 5% between 1979 and 1980.

The other assumption was the neglect of gradient and curvature drifts in solar latitude, which would allow cosmic-ray particles of a particular charge to enter the heliosphere over the solar poles and be transported across magnetic field lines and eventually out into interplanetary space along the ecliptic. Particles of opposite charge would travel in the reverse direction. Drifts were precluded by using a model in one space dimension only. I did this for two reasons: The first is that analysis of space probe data reveals no significant flux of particles coming in from the sunward side (see section I and references therein). The other was the presence of one or more changes in magnetic polarity over a full hemisphere of the Sun(north or south)during solar maximum. These are the "coronal holes," regions of unipolar magnetic field stretching from the Sun out into interplanetary space [see, e.g.,

Hundhausen et. al., 1981]. Since the direction of particle drifts depends on both the sign of a particle's charge as well as the sign of the magnetic field's polarity (eqn. (1), Section II), the existence of these regions suggested that large-scale drifts in latitude are cancelled by numerous small regions of randomly varying polarity.

The neglect of these drifts allowed me to ignore the difference in electrical charge between protons and antiprotons, and to use the known modulation of the protons to infer the modulation of the antiprotons, as detailed below. But first let us look briefly at an alternative solution to the transport equation for cosmic rays, provided by the so-called "force-field" approximation.

Force-field Approximation

At sufficiently high cosmic-ray energies, Gleeson & Axford [1968] have shown that the differential radial streaming, $\underline{S}$ (density of cosmic-ray particles passing through unit area in unit time), can be neglected. The cosmic-ray transport equation (eqn. 1, sec. I) then reduces to a form of Liouville equation. This is equivalent to combining convection-diffusion and energy losses of cosmic rays into an approximate heliocentric "force field" or an equivalent potential.

A simple derivation of the force-field solution can be attributed to Fisk *et. al.* [1973]. By neglecting the streaming in the equation of transport (eqn. 1, sec. I), I obtain

$$v \frac{\partial f}{\partial r} + v \frac{VP}{3\kappa} \frac{\partial f}{\partial P} \cong 0 \qquad (1)$$

where "f" is the omni-directional cosmic-ray distribution function averaged over particle direction, "V" is the solar wind speed; "κ" is the radial diffusion coefficient; "r" is the heliocentric radius; "P" is the particle rigidity (= pc/q, where "p" is the particle momentum, "q" is its charge and "c" is the speed of light); and "v" is the speed of the cosmic-ray particle. "VPv/3κ" is the equivalent one-dimensional "force" referred to earlier.

The solution to (1) can be expressed as

$$f = F[P'(P,r)] \qquad (2)$$

where F(P) is the interstellar distribution function, i.e., f(P) at the boundary of the Sun's modulation region (r=R). The function P'(P,r) represents characteristic curves on which "f" is constant. These contours result from (1) by integrating

$$dP = \frac{VP}{3\kappa}\, dr \qquad (3)$$

with the boundary condition P'=P at r=R. Equation (3) can be integrated to solve for "P'" which can be in turn used to solve for "f" using (2). I will now describe the numerical method used to solve for the proton modulation and give the results for both methods.

Numerical Method

First I chose an interstellar proton spectrum used regularly in modulation studies:

$$f \propto (T_o^2 + p^2c^2)^{-1.88} / pc \qquad (4)$$

where "T_o" is the particle rest energy. This was the same form used in sec. I, where its validity was detailed. The diffusion coefficient used was

$$\kappa(cm^2/s) = 1.086 \times 10^{22} \beta \qquad T < 444 \text{ MeV}$$

$$\kappa(cm^2/s) = 1.975 \times 10^{22} \beta P \qquad T > 444 \text{ MeV} \qquad (5)$$

where "T" is the particle's kinetic energy, "P" is particle rigidity in units of GV and "β" is the ratio of particle velocity to speed of light. This function was chosen so that the steady-state numerical modulation solution [Fisk, 1971a; Perko & Fisk, 1983; section I, this thesis] fitted the 1980 proton spectrum observed at 1 AU [courtesy of W. R. Webber]. The boundary of the heliosphere was set at 100 AU and the solar wind speed "V" was set at a constant 400 km/s. The equation was integrated numerically from 20 down to 0.1 GeV.

Results

The results for protons are shown in the energy spectra of Figure 1. The values of the ordinate are expressed in units of differential intensity "j," the units measured by observationalists, where $j=p^2f$. The abscissa is particle energy in GeV. The top solid curve is the assumed interstellar proton spectrum. The lower two curves are the numerical modulation (dark) and the 1980 proton data (light). This shows that eqn. (5) correctly represented the diffusion coefficient for these protons. In Figure 2, the dark curves are the same interstellar spectrum and numerical modulation spectrum as in Figure 1; the light curve is the "force-field" solution. Noticeable divergence between the force-field and the numerical solution occurred only below about 100 MeV where the difference amounted to about 20-25%. In the case of the data involved here, the force-field solution probably works well enough above about 45 MeV. Assuming, then, identical modulation for the p^+'s and p^-'s, we can see how various hypothesized interstellar spectra are altered by the Sun's influence.

Figures 3, 4 and 5 used an interstellar spectrum which is a hyperbolic function closely shaped to that of the most common cosmic-ray antiproton models. They are used only to illustrate the amount and the character of a modulated spectrum and are not intended as plausible models to explain the observations. The use of an ordinary function simplified the problem.

Figure 3 is a graph based on a spectrum of similar magnitude to leaky-box models from, for example, Protheroe [1981]. The ordinate represents cosmic-ray differential intensity, the abscissa is energy in GeV. The upper curve is the interstellar spectrum, the lower curve is

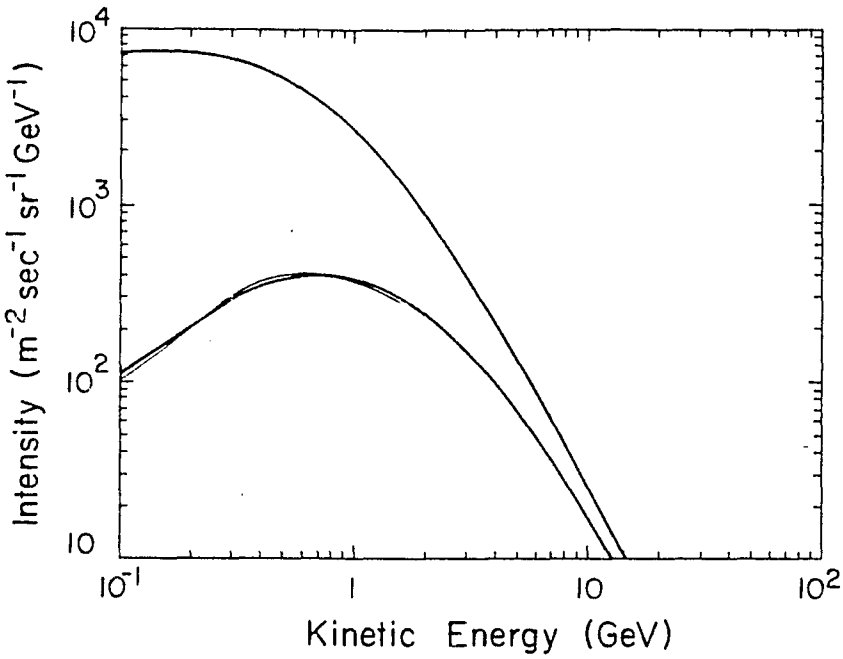

Figure 1. Proton intensity spectrum; upper(dark) curve is interstellar spectrum; diffusion coefficient was adjusted so that the calculated spectrum at 1 AU (lower dark curve) fitted 1980 proton data (courtesy of W. R. Webber) (lower light curve).

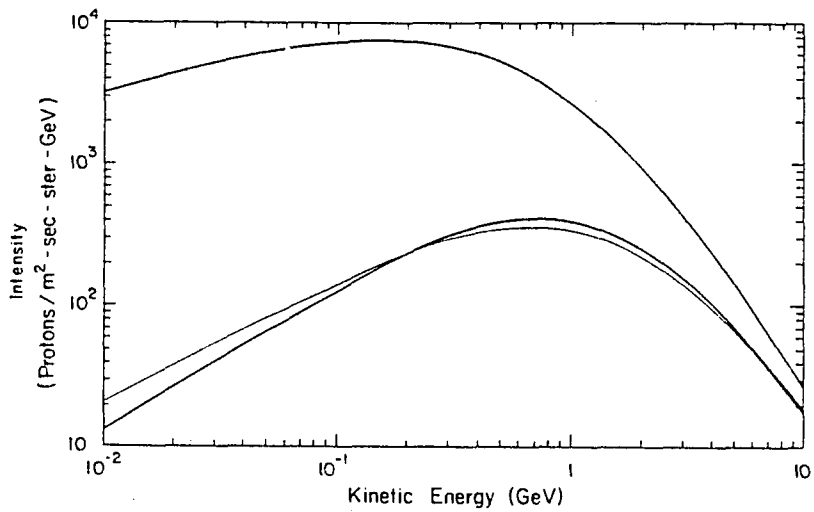

Figure 2. Interstellar and 1-AU proton intensity spectra (dark curves), same as in Figure 1; light curve is the "force-field" approximation of the 1-AU spectrum using the same diffusion coefficient as in Figure 1.

the spectrum numerically modulated as it appears at 1 AU. The datum marked "Bu" is Buffington et. al.'s measurement, "Bo" is Bogomolov et. al.'s, and the four marked "G" are from Golden et. al. (Figures 4 and 5 are arranged the same way.) Since Golden's and Bogomolov's data were reported solely in p^-/p^+ ratios, the differential intensities "G" and "Bo" plotted here were calculated by multiplying their ratios by the 1980 proton intensity (Figure 1) at the appropriate energy. This conversion should be accurate enough for my purposes since the proton spectrum should not change radically in the span of a year (1979-80) during solar maximum, as explained above. A look at this figure shows that this model clearly satisfied none of the observations.

Figure 4 used the same interstellar spectrum as Figure 3 multiplied by 9. The modulated solution passed through all of the data except for Buffington's. In order to approach Buffington's observation, I had to multiply the interstellar spectrum by at least 90 or so. This scaling was done in Figure 5. A comparison of Figures 4 and 5 clearly shows that an unusually steep slope at the high-energy end of the spectrum is required to pass through all of the data illustrated, when solar modulation is done properly. This distortion of the galactic spectrum is difficult to justify, since the high-energy slopes of a wide variety of interstellar models are consistently the same. (See, for example, the collection exhibited in Figure 1 of Tan & Ng [1983].)

Since most of the experimenters cited here reported their results in p^-/p^+ ratios, one may legitimately pose the question: Does the use in this theory of p^-/p^+ ratios instead of p^- intensities change the situation? Figure 6 graphs the p^-/p^+ ratios for the same interstellar spectra used in Figures 1 and 3. All other parameters were kept

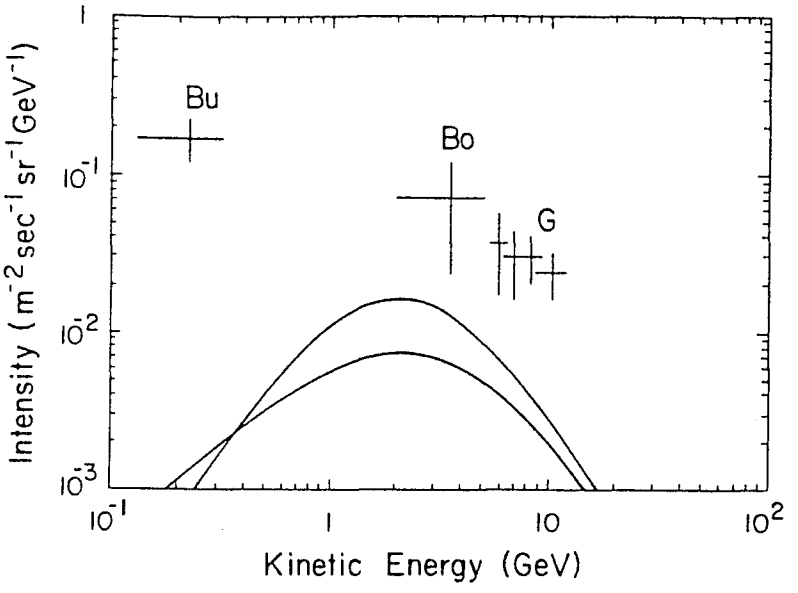

Figure 3. Hypothetical interstellar spectrum (upper dark curve) with modulated spectrum at 1 AU (lower dark curve) using same diffusion coefficient as in Figures 1 and 2; "Bu" indicates datum of Buffington et. al.; "Bo" is datum of Bogomolov et. al. and "G" is data of Golden et. al.

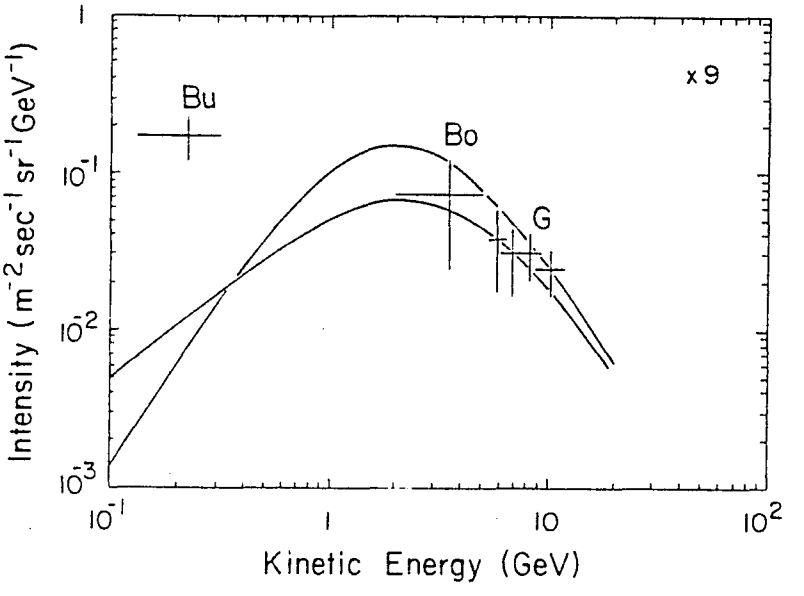

Figure 4. Same as Figure 3 with interstellar spectrum multiplied by 9 and modulated curve calculated as before.

the same. In this picture, the upper dark curve is the modulated spectrum and the lower dark curve is the unmodulated one. The "force-field" solution is the light curve. As in Figure 3, this doesn't fit either. Multiplying the unmodulated p^- spectrum by 30 obtains Figure 7, which passed through Buffington's point, but skipped by the others, as in Figure 5. The reason that a factor of 30 is sufficient instead of the 90 in Figure 5 was that Buffington et. al. provided their own measure of the actual antiproton intensity, which was used in Figure 7. The proton intensity they measured at that energy differs from the one in Figure 1, hence the discrepancy. In any case, even accounting for this discrepancy, there was no help for this spectral shape.

Also, there is in Tan & Ng [1983] an attempt to fit all the data with a so-called "revised closed galaxy" model. Figure 8 shows the most intense interstellar spectrum in the range they calculated. The authors made no attempt to modulate their galactic spectrum. But their distribution, when correctly modulated, does not come close to Buffington's datum.

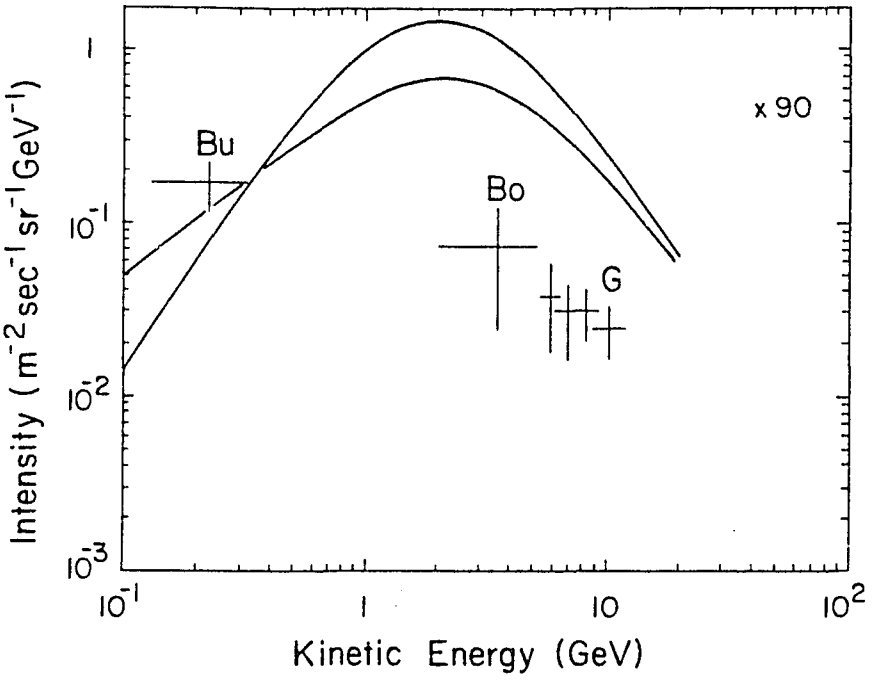

Figure 5. Same as Figure 4 with interstellar spectrum multiplied by 90.

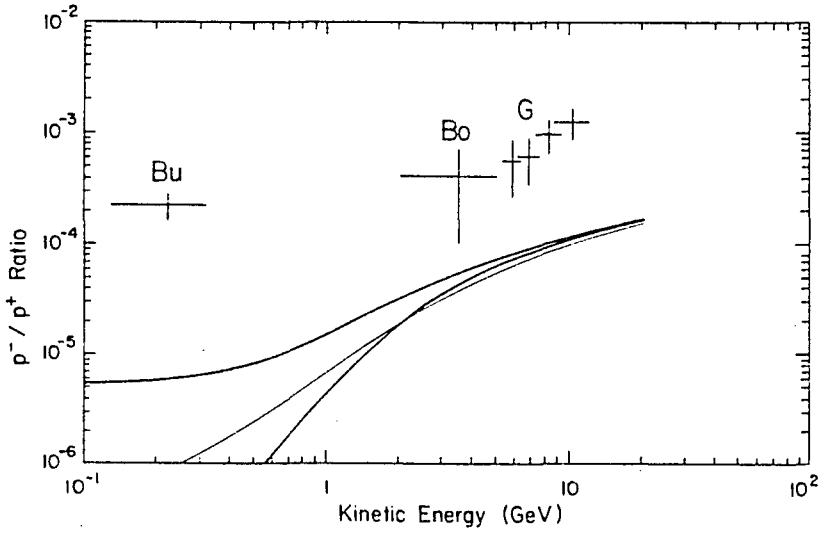

Figure 6. Kinetic energy versus antiproton/proton ratios, combining the numbers from Figures 1 and 3.

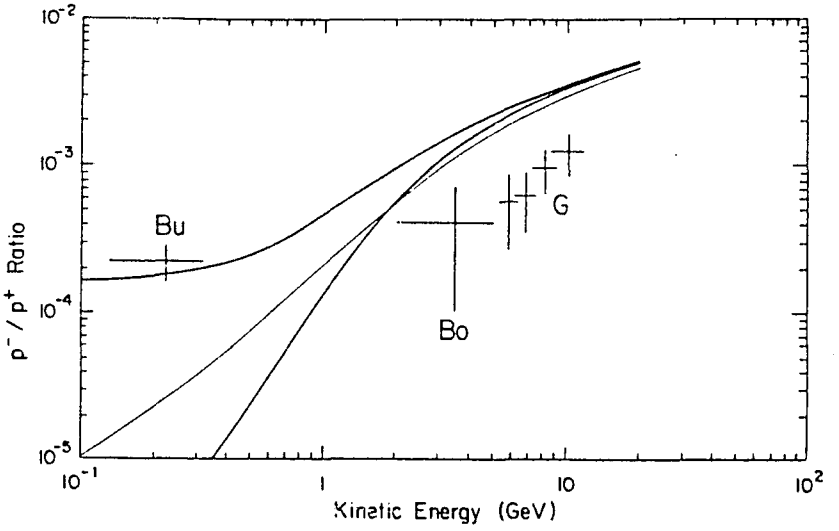

Figure 7. Same as Figure 6 with the antiproton interstellar spectrum multiplied by 30.

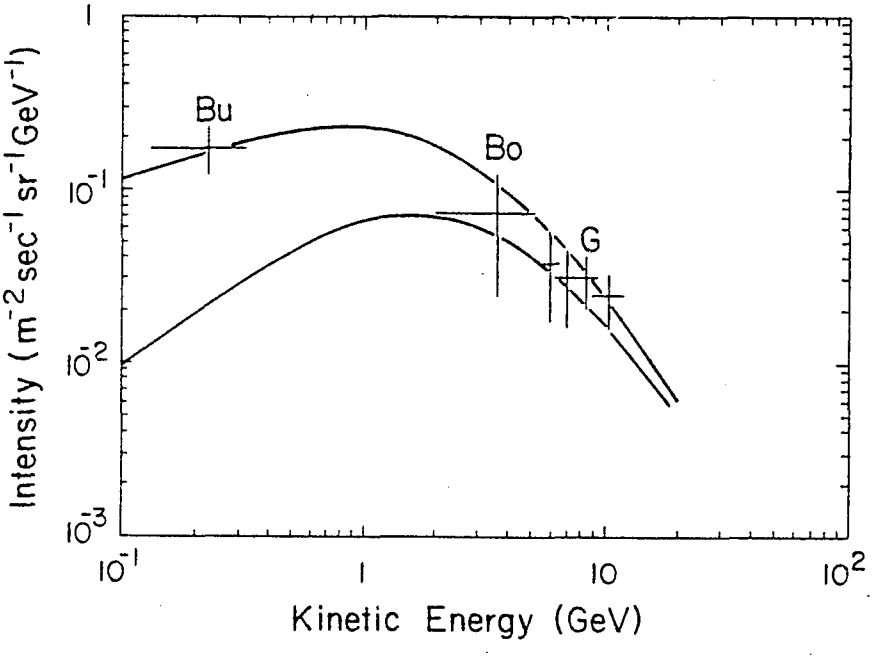

Figure 8. Top curve if the maximum amplitude antiproton spectrum of Tan & Ng's "revised closed galaxy" model; lower is the modulated curve at 1 AU for the model used in this section.

Conclusion

Careful attention to solar modulation is necessary when interpreting cosmic-ray data taken at 1 AU (or anywhere in the heliosphere). This includes any cosmic rays measured at less than about 10 GeV at Earth. The most rigorous results from current theory derive from numerical calculations, although force-field solutions may suffice for some applications. For cosmic-ray antiprotons specifically, correct application of solar modulation puts recent data at odds with current theories of interstellar antiproton production and propagation by forcing an unacceptably steep slope in the interstellar spectrum on the high-energy side.

IV. INFLUENCE OF A TERMINATION SHOCK ON ENERGY-LOSS CALCULATIONS IN THE SOLAR WIND

Introduction

The adiabatic loss of energy by galactic cosmic rays in the expanding solar wind has been part of solar modulation theory for some time [Parker, 1965, 1966]. One of the principal effects of this deceleration was realized by Goldstein et. al. [1970] and Gleeson & Urch [1971]: Interstellar protons less than around 100 MeV are so reduced in intensity by the time they reach 1 AU that they are rendered practically unobservable. Particles heavier than protons with higher rigidity are less modulated; their exclusion occurs at lower energies (60-80 MeV/nucleon). We are far more likely to see, at these low energies, particles cooled down from higher energies, since they have a better chance of making it upstream in the solar wind. Thus, we have insufficient data with which to judge the effects of low-energy particles in interstellar space (for example, on the energy density or ionization state).

Another by-product of the adiabatic deceleration theory is an explanation for observations of the He to C+N+O intensity ratio taken during an earlier solar cycle [Garcia-Munoz, 1973]. This ratio stays constant down to low energies even though C, N and O should suffer greater ionization losses in the interstellar medium, and thus have their densities depressed in local interstellar space. If these cosmic rays traverse sufficient material to be destroyed by spallation and create the interstellar Li, Be and B observed, the interstellar

He/(C+N+O) ratio at energies less than about 100 MeV should rise well above the observed ratio [Mason, 1972]. Using adiabatic deceleration, it is clear that any He and C+N+O, measuring less than about 100 MeV/nucleon at 1 AU, originated at much higher energies, where ionization loss is negligible.

Another direct result of adiabatic deceleration is the consistent slope of low-energy cosmic-ray spectra near Earth. Indeed, Rygg & Earl [1971] found that the slope of the low-energy proton spectrum is always near unity throughout the solar cycle; that is, the differential intensity j is proportional to T, the kinetic energy. This has been found true of other species as well, such as ^{2}H and ^{3}He [Teegarden et. al., 1975].

The reason for this can be seen directly from the steady-state version of eqn. (1), Section I:

$$0 = \frac{1}{r^2}\frac{\partial}{\partial r}(r^2\kappa\frac{\partial f}{\partial r}) - V\frac{\partial f}{\partial r} + \frac{1}{r^2}\frac{\partial}{\partial r}(r^2V)\frac{p}{3}\frac{\partial f}{\partial p} \qquad (1)$$

In general, particles on the low-energy side of the near-Earth spectrum have been cooled down in interplanetary space, so the spectral shape there depends more on interplanetary processes than on processes in interstellar space. This equation describes those interplanetary processes. To show this in an approximate way, note that cooled particles come from higher-energy ones which are not as heavily modulated; they are thus more evenly distributed in radial distance [e.g., McKibben et. al., 1973]. So we can approximate the radial gradient

$$\partial f/\partial r << f/r$$

in eqn. (1). This also assumes that the diffusion coefficient κ decreases with decreasing energy. Most successful forms of κ do this. All that is then left of eqn. (1) is

$$\partial f/\partial P \cong 0 \ ,$$

where "P" can be the rigidity as well as the momentum ($P \propto p$). This means f is constant in momentum. Since $j=p^2f$, $j \propto P^2$. The relation between rigidity and kinetic energy is

$$T = (T_o^2 + p^2c^2)^{\frac{1}{2}} - T_o \quad \text{(GeV)}$$

where "T_o" is the rest-mass energy. For $pc<<T_o$

$$T \cong p^2c^2/(2T_o)$$

$$p^2c^2 \cong 2TT_o \ .$$

So

$$j \propto T \ .$$

Note that this also works in the two-dimensional(r-θ) case if the latitudinal gradients are small [see Fisk, 1979].

It has long been felt that a termination shock exists in the solar wind [see, e.g., Axford et. al., 1963]. The density of the solar wind decreases as $1/r^2$ in the spherical cavity with a commensurate decrease in its ram pressure. Spacecraft observations have also shown the solar wind speed virtually constant out to large distances [Collard et. al., 1982]. The result of this is that the ram pressure of the solar wind eventually decreases until it reaches the pressure of the interstellar medium, at which point a shock should form; the supersonic wind becomes subsonic. Unless circumstances in the outer solar system are far different from most current conceptions, we do expect this shock to exist. If so, we also expect the sudden solar wind velocity change to compress and accelerate the particles which reach the shock front, including cosmic rays injected from the local interstellar medium. Work by Fisk [1971b] followed by others indeed shows that such shocks are efficient accelerators of particles. Diffusion theory includes

multiple passes through the shock front (hence multiple accelerations) by the particles, caused by scattering centers on either side, confining the particles to the vicinity of the shock for some time. In fact, shocks now appear to be a principal candidate for the acceleration of cosmic rays in interstellar space [see the review by Drury, 1983, and references therein].

A few analytical attempts have been made to solve the transport equations for cosmic rays inside the heliosphere with a termination shock, convection-diffusion, and adiabatic deceleration [e.g., Jokipii, 1968; Webb et. al., 1983]. A perturbative solution was described by Drury [1983]. All of these solutions use a diffusion coefficient constant in momentum, which is known to be unrealistic. I wish to examine in a more precise way whether the presence of a termination shock affects the earlier conclusions on adiabatic deceleration. Specifically, can low-energy particles in the interstellar medium reach the shock front, receive a boost in energy, then be adiabatically decelerated to their original energy. In other words, what is the interstellar energy of cosmic rays observed near Earth at low energies?

This section takes a further step toward answering the question by using a spherically-symmetric, steady-state, numerical cosmic-ray transport code, similar to the one used in Section I. The difference lies in the treatment of the boundary condition at the outer edge of the heliosphere. In the first section I simply assumed a constant cosmic-ray spectral distribution there for all time. This served as a constant and exclusive source of particles, while any sources and sinks were shut off at r=0. In this section, a sharp decrease in solar wind

velocity at the boundary forms a shock, while downstream of the shock, conditions must be specified in detail.

The tactic in this section is to derive at the shock a steady-state solution for cosmic-ray behavior with convection and diffusion, but neglecting adiabatic deceleration downstream and upstream. (In this section, "downstream" will refer to space outside the shock while "upstream" will refer to space inside the heliosphere.) This will maximize the acceleration of particles at the shock. This solution will then be used as the boundary condition at the edge of the heliosphere for a steady-state, numerical modulation solution, including adiabatic deceleration inside the heliosphere.

The results clearly show that even with the most favorable treatment of the shock acceleration given here, any increase in the low-energy particles at 1 AU due to the shock is still overwhelmed by higher-energy particles brought down in energy inside the heliosphere. The low-energy spectrum, therefore, is dominated by these decelerated cosmic rays.

Technique

Consider a termination shock at some distance r=R. When r<R, the spherically-symmetric transport equation for cosmic rays holds, as in section I, except that is is now time-independent:

$$0 = \frac{1}{r^2}\frac{\partial}{\partial r}(r^2\kappa\frac{\partial f}{\partial r}) - V\frac{\partial f}{\partial r} + \frac{1}{r^2}\frac{\partial}{\partial r}(r^2V)\frac{p}{3}\frac{\partial f}{\partial p} \qquad (1)$$

where "f" is the density of particles in phase space averaged over particle direction; "f" is related to the particle differential intensity "j" by $j = p^2 f$. Also, "r" is the heliocentric radial distance, "V" the solar-wind speed, "p" the particle momentum, and "κ" the diffusion coefficient for radial propagation. In this model, I took the upstream solar wind constant, as in the other sections. I assumed that the thickness of the shock is small compared to the scale of the radial step used in the numerical computation. With that, the Rankine-Hugoniot relations held, and conditions on either side of the shock were different, but constant in time. On either side, then, we can use the adiabatic equation of state for the solar wind:

$$P\rho^{-\gamma} = \text{constant} \quad ,$$

where "ρ" is the density, "P" is in this instance the pressure and "γ" is the adiabatic index. Using this and the jump conditions at the shock, we have

$$H < (\gamma+1)/(\gamma-1) \quad ,$$

where "H" is the ratio of the flow velocity outside the shock to flow velocity inside [Boyd & Sanderson, 1969]. For an assumed monatomic gas, $\gamma=5/3$; so r=1/4.

Now look for a moment at the mass continuity equation outside the shock:

$$\frac{\partial \rho}{\partial t} + \nabla \cdot \rho \underline{V} = 0 \quad .$$

We know that density is nearly constant in a subsonic gas; thus ρ is a constant downstream. So, in the spherically-symmetric case, the previous equation becomes

$$\frac{\partial}{\partial r}(r^2 \rho V) = 0 \quad .$$

Since ρ and V are constants, V must go as $1/r^2$ outside the shock. We must then substitute the expression $(V'R^2/r^2)$ for the flow velocity downstream of the shock. V' is a constant equal to V/4 for the strong shock case discussed above. Since V' goes as $1/r^2$, we also see that the last term in eqn. (1) drops out in the downstream region; that is, there is no adiabatic deceleration outside the shock.

Referring to values outside the shock as primed variables, the equation for r>R is, after the above considerations,

$$0 = \frac{1}{r^2} \frac{\partial}{\partial r}(r^2 \kappa' \frac{\partial f'}{\partial r}) - \frac{V'R^2}{r^2} \frac{\partial f'}{\partial r} \qquad (2).$$

Equation (2) can be integrated once to obtain

$$r^2 \kappa' \frac{\partial f'}{\partial r} - V'R^2 f' = -C \qquad (3),$$

where "C" is the constant of integration. The solution of this equation is

$$f' = \frac{C}{V'R^2} + D \exp[-I] \qquad (4)$$

where

$$I \equiv \int_r^\infty \frac{V'R^2}{r^2 \kappa'} dr \qquad (5).$$

At $r = \infty$, $f' = f_o$, the constant interstellar spectrum. Substituting this boundary condition into (4) yields

$$f' = f_o + D [\exp(-I) - 1] \qquad (6).$$

Furthermore, at the shock boundary (r=R), the differential streaming (number of cosmic rays crossing unit area per unit time) must match from either side. Hence

$$-\frac{V}{3} p \frac{\partial f}{\partial p} - \kappa \frac{\partial f}{\partial r} = -\frac{V'}{3} p \frac{\partial f}{\partial p} - \kappa' \frac{\partial f'}{\partial r} \qquad (7).$$

(A prime on the first term on the right side is unnecessary since "f" is continuous across the boundary.) Differentiating (6) once, substituting into (7) and collecting terms gives

$$\kappa \frac{\partial f}{\partial r} = -\frac{(V - V')}{3} p \frac{\partial f}{\partial p} + V' D \exp[-I] \qquad (8).$$

Also from (6),

$$D = (f' - f_o) / (\exp[-I] - 1) \qquad (9).$$

Let

$$\chi \equiv [1 - \exp(I)]^{-1} \qquad (10).$$

Thus,

$$D = (f - f_o)\chi / \exp[-I] \qquad (11),$$

using, again, f=f' at the shock. Finally, combining (11) and (8),

$$\kappa \frac{\partial f}{\partial r} = -\frac{(V - V')}{3} p \frac{\partial f}{\partial p} + V'\chi(f - f_o) \qquad (12)$$

at r=R.

Next, let us look at a way to maximize the acceleration of cosmic rays at the shock. One way to do this might be to solve an equation which details cosmic-ray behavior at a shock boundary, assuming no adiabatic deceleration downstream or upstream of the shock. This amounts to allowing particles to come in from infinity, where a constant interstellar spectrum is maintained, be accelerated by the shock front, make their way upstream, and be convected back downstream, all without losing energy. The neglect of adiabatic deceleration downstream can be

well justified by noting the large size of the solar cavity in this model (100 AU). At this distance, the shock is almost planar, a situation in which no divergence of flow takes place, no $\nabla \cdot \underline{V}$ in the final term of eqn. (1), and therefore no adiabatic deceleration in the region close to the shock.

Furthermore, let us rewrite eqn. (1):

$$0 = \frac{1}{r^2} \frac{\partial}{\partial r}(r^2 \kappa \frac{\partial f}{\partial r} - r^2 V f) + \frac{Vf}{r} + \frac{2Vp}{3r} \frac{\partial f}{\partial p} \qquad (13).$$

Low-energy particles should scatter more easily than high-energy ones in the solar wind, since their diffusion coefficient is smaller. They should not move far upstream, and thus remain closer to the shock. Their intensity would drop off quickly, creating a large radial gradient. Thus,

$$\frac{\partial f}{\partial r} >> \frac{f}{r} \qquad (14).$$

This presumption, coupled with the near-planar shape of the shock, at least locally, should keep these cosmic rays from losing too much energy in the solar wind.

Using (14) to neglect terms in f/r in eqn. (13), we get

$$\frac{\partial}{\partial r}(r^2 \kappa \frac{\partial f}{\partial r} - r^2 V f) = 0 \qquad (15)$$

or

$$\kappa \frac{\partial f}{\partial r} = Vf \qquad (16)$$

as a valid solution inside the solar cavity, near the shock. Substitute (16) into (12):

$$Vf = \frac{-(V-V')}{3} p \frac{\partial f}{\partial p} + V' \chi (f - f_o) \qquad (17)$$

or

$$\frac{df}{dp} = \frac{3}{p(V'-V)} [Vf - V'\chi(f-f_o)] \qquad (18)$$

at r=R. This equation can be solved numerically for f(R,p). The result is a spectrum of particles at the shock front which can be used as a source of particles for a time-independent, numerical modulation calculation, identical to the initial time-step computation in Section I and the solution of Fisk [1971a].

The diffusion coefficient was the same on both sides of the shock and was taken from Section I:

$$\kappa = 4.3\ \beta\ (2 + P^2)\ 10^{21}\ cm^2/s \qquad (19)$$

where "P" is the rigidity and "β" is particle velocity divided by the speed of light. This form was justified in Section I on both theoretical and observational grounds. The interstellar spectrum placed at infinity was a series of essentially monoenergetic peaks in the form of thin gaussians,

$$f_o = A\ \exp[-B(P-P_o)^2] \qquad (20)$$

where "A" and "B" are constants and "P_o" is the location of the gaussian peak, a constant for any given modulation solution. These were used to track the behavior of particles from narrow energy bands. The shock was located at R=100 AU. "V" was set to a constant equivalent to 400 km/s, so a maximum strength shock required that V'=100 km/s. Since V', R, and κ' were independent of radius, eqn. (5) could be easily integrated to yield I = V'R/κ', where I set κ'= κ, as noted above. At r=0, I used the same condition as in section I; namely, that the differential streaming at the origin is zero:

$$-\frac{V}{3}\ p\ \frac{\partial f}{\partial p} - \kappa\ \frac{\partial f}{\partial r} = 0 \qquad (21).$$

Again, this prevents spurious particles from entering the modulation region at the origin.

Results

A characteristic result of this model is shown in Figure 1. The thin gaussian at 0.05 GeV is the injection spectrum at infinity. The next lower curve is the spectrum at the outer boundary. The lowest curve is the distribution of particles at 1 AU. In a one-dimensional, planar shock calculation, we expect a power law distribution of accelerated particles of the form $f \propto p^{-4}$ for a strong shock in a monatomic gas, given a monoenergetic injection spectrum [see, e.g., Drury, 1983]. This figure shows a power law, just above 0.05 GeV, formed by the accelerated particles. However, at higher energies on the outer-boundary spectrum, there is a visible loss in intensity caused by leakage into the interstellar medium. This is due to the second term in the boundary condition, eqn. (17), which allows diffusion downstream. The average kinetic energy for the particles at 1 AU has increased to about 0.38 GeV, though the maximum intensity has fallen off by more than a factor of 100 from the intensity at the outer boundary. Note also the spread in energy in the 1 AU curve, with a significant portion of the spectrum at high energies.

I now come to the question of whether this enhancement of particles from the 50 MeV interstellar spectrum could be visible near Earth. I can investigate this by mixing in particles from other points on the interstellar proton spectrum. Figure 2 has three other monoenergetic peaks for the interstellar injection spectrum in addition to 0.05 GeV: 0.2, 0.5 and 1.0 GeV. The maxima of all four of these peaks were normalized to the shape of the power-law, interstellar proton spectrum used in Sections I, II and III (see Figure 3). The lower dark curves labelled 1 through 4 are the modulated spectra at 1 AU resulting

from the corresponding gaussian sources, also marked 1 through 4. The light curve is the sum of the four modulated curves. It overwhelms the particles which had an original energy of 0.05 GeV by factors ranging from 30 to 100. The low-energy particles were easily lost by the addition of only a few narrow high-energy bands. We see just the high-energy particles decelerated in interplanetary space. Even though there is an energy gain, the modulation was too great; the low-energy cosmic rays are still excluded from the inner solar system while the high-energy ones fill in from above.

To complete this demonstration, Figure 3 shows the entire interstellar proton spectrum (top curve), a power law in total energy with a spectral index of 2.6 (see Section I). The lower dark curve is the modulated curve at 1 AU with the shock present at the outer boundary, the lower light curve is the same without the shock. In both the shocked and the unshocked cases, the downstream modulation had to be kept the same for a clear comparison between the two. Since the downstream flow speed V', originally V/4 in the shocked case, had to be multiplied by four to get the unshocked case, a glance at eqn. (2) shows that multiplying κ' by four leaves the equation, and therefore the downstream modulation, unchanged. The difference between the two situations, then, lies exclusively in the presence or absence of the shock front.

The unshocked spectrum at 1 AU is about 1.7 times higher than the shocked one at energies less that about 200 MeV. Even so, when the shock process is maximized, the spectrum did not rise significantly, within the uncertainties of the parameters, particularly those in the

outer solar system not yet measurable: the downstream diffusion coefficient, the strength of the shock, etc.

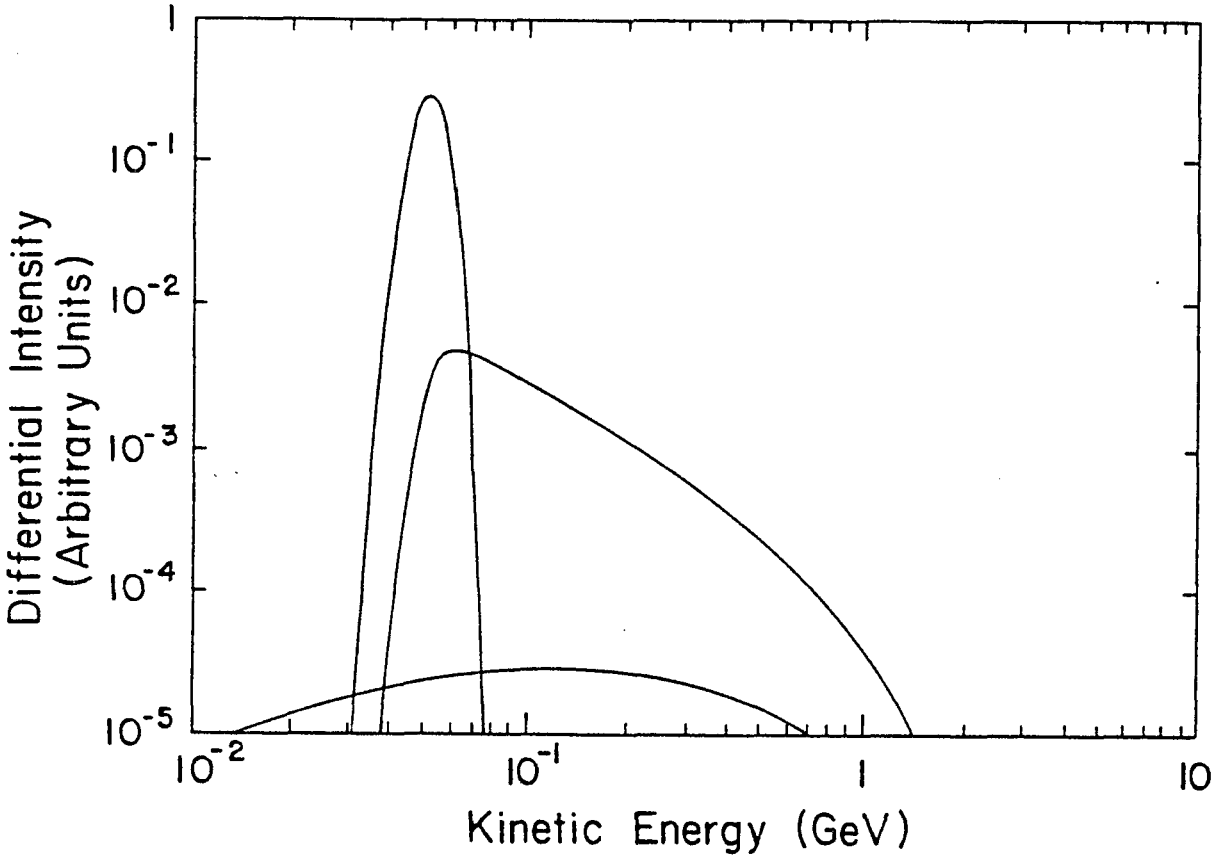

Figure 1. Narrow top curve is 50 MeV interstellar injection spectrum; next lower curve is the spectrum of particles at the shock boundary, with the modified power spectrum of accelerated particles; lowest curve is the modulated spectrum at 1 AU.

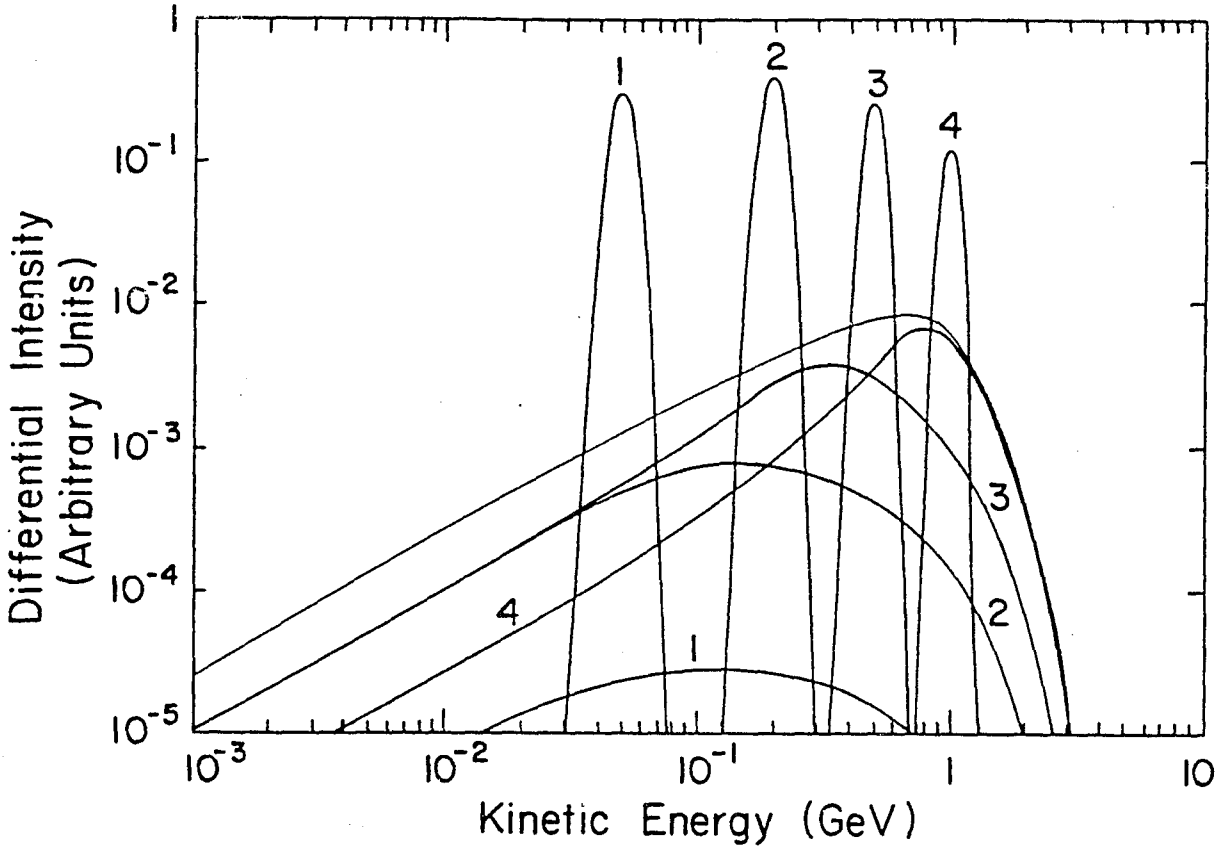

Figure 2. Upper curves are four sets of injection spectra: 50, 200, 500 and 1000 MeV (labelled 1 through 4); lower four dark curves (also labelled 1-4) are the corresponding modulated spectra at 1 AU; lower light curve is the sum of modulated curves 1-4.

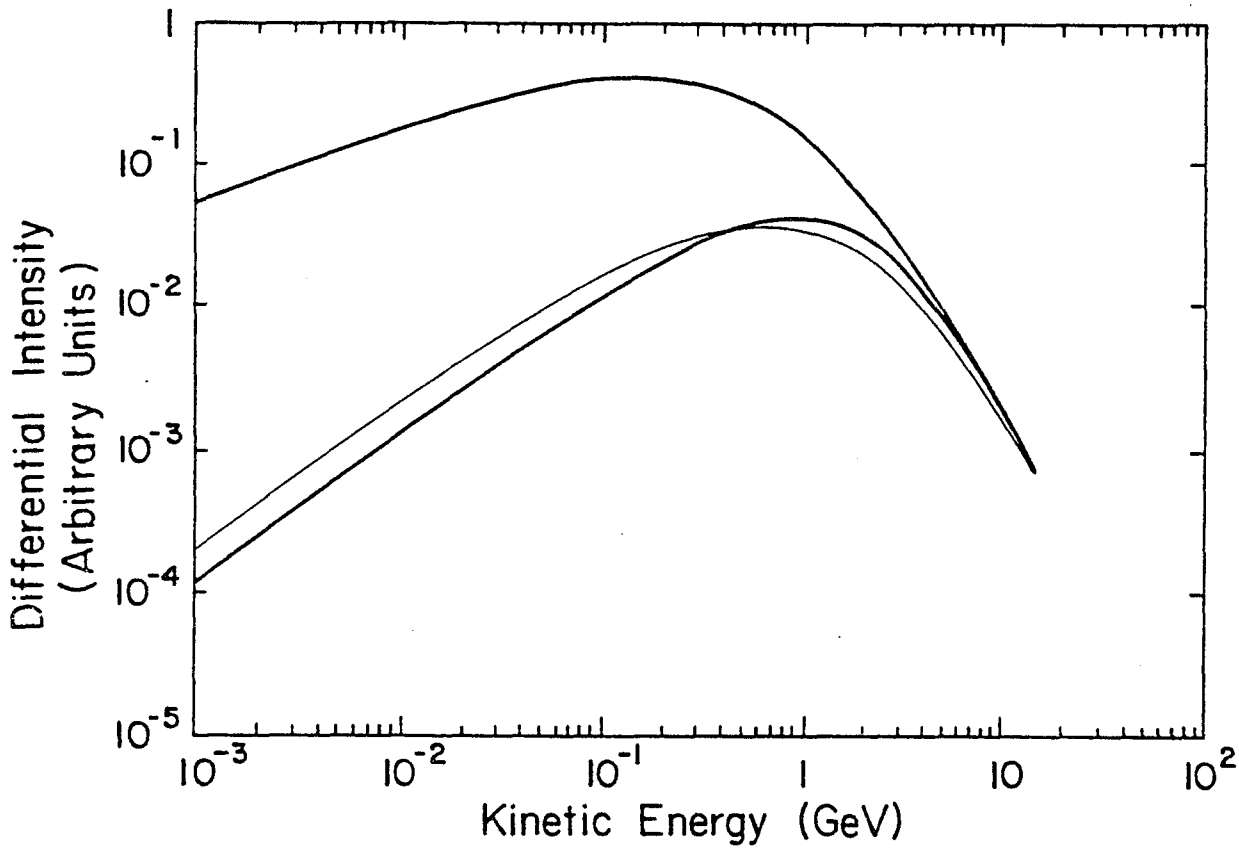

Figure 3. Top curve is unnormalized interstellar proton spectrum injected from infinity; lower light is modulated spectrum at 1 AU without a shock; lower dark is modulated spectrum at 1 AU with a shock.

Discussion

I have presented a technique here that can maximize the acceleration of galactic cosmic rays at a termination shock on the outer edge of the heliosphere. This was done by letting particles interact with the shock without letting them lose energy by adiabatically decelerating in the upstream solar wind, thus building up a steady state at the the shock boundary. This steady-state was then used in solving a spherically-symmetric, numeric, steady-state modulation equation with adiabatic deceleration.

This method can only be justified for low-energy particles, since their mean free paths in the solar wind are much smaller than high-energy particles. This means that they are more easily scattered and are more likely to remain in the vicinity of the shock and not suffer adiabatic deceleration over any great distance.

From the calculations here, I think we can conclude fairly strongly that the effect of a termination shock on the near-Earth distribution of low-energy particles is insignificant compared to the effect of particles cooled down from much higher energies. This means that previous conclusions [Webb et. al., 1983], remain unchanged and that most modulation calculations may proceed free of any complications from a termination shock.

LIST OF REFERENCES

Axford, W. I., A. J. Dessler and B. Gottlieb, Termination of solar wind and solar magnetic field, Astrophys. J., 137, 1268, 1963.

Bastian, T. S., R. B. McKibben, K. R. Pyle and J. A. Simpson, Gradients of galactic cosmic rays and anomalous helium to greater than 23 AU during the increase of solar modulation in 1978-80, Proc. Int. Cosmic Ray Conf. 17th (Paris), 10, 88, 1981.

Bogomolov, E. A., N. D. Lubyanaya, V. A. Romanov, S. V. Stepanov, and M. S. Shulakova, Galactic antiprotons of 2-5 GeV energy, Proc. Int. Cosmic Ray Conf. 17th (Paris), 9, 146, 1981.

Boyd, T. J. M., and J. J. Sanderson, Plasma Dynamics, Ch. 6, Barnes & Noble, New York, 1969.

Buffington, A., S. M. Schindler, and C. R. Pennypacker, A measurement of the cosmic-ray antiproton flux and a search for antihelium, Astrophys. J., 248, 1179, 1981.

Burger, J. J., and B. N. Swanenburg, Energy dependent time lag in the long-term modulation of cosmic rays, J. Geophys. Res., 78, 292, 1973.

Burlaga, L. F., R. Schwenn and H. Rosenbauer, Dynamical evolution of interplanetary magnetic fields and flows between 0.3 AU and 8.5 AU: entrainment, Geophys. Res. Lett., 10, 413, 1983.

Collard, H. R., J. D. Mihalov and J. H. Wolfe, Radial variation of the solar wind speed between 1 and 15 AU, J. Geophys. Res., 87, 2203, 1982.

Cummings, A. C., E. C. Stone, and R. E. Vogt, Interstellar electron spectrum from the galactic non-thermal radio emission, Proc. Int. Cosmic Ray Conf. 13th (Denver), 1, 335, 1973.

Diaz, J. B., Partial differential equations, in Handbook of Automation, Computation, and Control, ed. E. M. Crabbe, S. Ramo and D. E. Wooldridge, pp. 14-64 to 14-90, John Wiley, New York, 1958.

Drury, L. O'C., An introduction to the theory of diffusive shock acceleration of energetic particles in tenuous plasmas, Rep. Prog. Phys., 46, 973, 1983.

Evenson, P., M. Garcia-Munoz, P. Meza, K. R. Pyle, and J. A. Simpson, A quantitative test of solar modulation theory: The proton, helium and electron spectra from 1965 through 1979, Astrophys. J., 275, L15, 1983.

Evenson, Paul, and Peter Meyer, Solar modulation of cosmic ray electrons 1978-1983, J. Geophys. Res., 89, 2647, 1984.

Fisk, L. A., Solar modulation of galactic cosmic rays, 2, J. Geophys. Res., 76, 221, 1971a.

Fisk, L. A., Increases in the low-energy cosmic ray intensity at the front of propagating interplanetary shock waves, J. Geophys. Res., 76, 1662, 1971b.

Fisk, L. A., Solar modulation of galactic cosmic rays, 4. Latitude-dependent modulation, J. Geophys. Res., 81, 4646, 1976.

Fisk, L. A., The interactions of energetic particles with the solar wind, in Solar System Plasma Physics, Vol. 1, ed. by E. N. Parker, C. F. Kennel and L. J. Lanzerotti, North-Holland, New York, p.177, 1979.

Fisk, L. A., and W. I. Axford, Solar modulation of galactic cosmic rays, 1, J. Geophys. Res., 74, 4973, 1969.

Fisk, L. A., M. A. Forman and W. I. Axford, Solar modulation of galactic cosmic rays, 3. Implications of the Compton-Getting coefficient, J. Geophys. Res., 78, 995, 1973.

Forbush, S., On world-wide changes in cosmic ray intensity, Phys. Rev., 54, 975, 1938.

Garcia-Munoz M., Cosmic ray charge composition ($Z \leq 28$), Proc. Int. Cosmic Ray Conf. 13th (Denver), 5, 3513, 1973.

Gleeson, L. J., and W. I. Axford, Cosmic rays in the interplanetary medium, Astrophys. J., 149, L115, 1967.

Gleeson, L. J., and W. I. Axford, Solar modulation of galactic cosmic rays, Astrophys. J., 154, 1011, 1968.

Gleeson, L. J., and I. H. Urch, Energy loss and modulation of galactic cosmic rays, Astrophys. Space Sci., 11, 288, 1971.

Gloeckler, G., and J. R. Jokipii, Low-energy cosmic-ray modulation related to observed interplanetary magnetic field fluctuations, Phys. Rev. Letters, 17, 203, 1966.

Golden, R. L., B. G. Mauger, S. Nunn, and S. Horan, Energy dependence of the $\bar{p}/p$ ratio in cosmic rays, Astrophys. Lett., 24, 75, 1984.

Goldstein, M. L., L. A. Fisk and R. Ramaty, Energy loss of cosmic rays in the interplanetary medium, Phys. Rev. Letters, 25, 832, 1970.

Hatton, C. J., Solar flares and the cosmic ray intensity, Solar Phys., 66, 159, 1980.

Holzer, T. E., The solar wind and related astrophysical phenomena, in Solar System Plasma Physics, Vol. 1, ed. by E. N. Parker, C. F. Kennel and L. J. Lanzerotti, North-Holland, New York, p. 146, 1979.

Hundhausen, A. J., Coronal Expansion and Solar Wind, p. 175, Springer-Verlag, New York, 1972.

Hundhausen, A. J., R. T. Hansen, and S. F. Hansen, Coronal holes during the sunspot cycle: Coronal holes observed with the Mauna Loa K-coronameters, J. Geophys. Res., 86, 2079, 1981.

Isenberg, P. A., and J. R. Jokipii, Gradient and curvature drifts in magnetic fields with arbitrary spatial variation, Astrophys. J., 234, 746, 1979.

Jokipii, J. R., Cosmic-ray propagation. I. Charged particles in a random magnetic field, Astrophys. J., 146, 480, 1966.

Jokipii, J. R., Cosmic-ray propagation. 2. Diffusion in the interplanetary magnetic field, Astrophys. J., 149, 405, 1967.

Jokipii, J. R., Acceleration of cosmic rays at the solar wind boundary, Astrophys. J., 152, 799, 1968.

Jokipii, J. R., Propagation of cosmic rays in the solar wind, Rev. Geophys. Space Phys., 9, 27, 1971.

Jokipii, J. R., and P. J. Coleman Jr., Cosmic ray diffusion tensor and its variation observed with Mariner IV, J. Geophys. Res., 73, 5495, 1968.

Jokipii, J. R., and E. N. Parker, Stochastic aspects of magnetic lines of force with applications to cosmic ray propagation, Astrophys. J., 155, 777, 1969.

Jokipii, J. R., and E. H. Levy, Effects of particle drifts on the solar modulation of galactic cosmic rays, Astrophys. J., 213, L85, 1977.

Jokipii, J. R., E. H. Levy, and W. B. Hubbard, Effects of particle drift on cosmic-ray transport. I. General properties, application to solar modulation, Astrophys. J., 213, 861, 1977.

Lee, M. A., and L. A. Fisk, The role of particle drifts in solar modulation, Astrophys. J., 248, 836, 1981.

Longair, M. S., High Energy Astrophysics, p. 111, Cambridge University Press, Cambridge, 1981.

Mason, G. M., Interstellar propagation of galactic cosmic-ray nuclei $2 \leq Z \leq 8$ in the energy range 10-1000 MeV per nucleon, Astrophys. J., 171, 139, 1972.

McDonald, F. B., J. H. Trainor, J. D. Trainor, J. D. Mihalov, J. H. Wolfe and W. R. Webber, Radially propagating shock waves in the outer heliosphere: the evidence from Pioneer 10 energetic particle and plasma observations, Astrophys. J., 246, L165, 1981a.

McDonald, F. B., N. Lal, J. H. Trainor, M. A. I. Van Hollebeke and W. R. Webber, The solar modulation of galactic cosmic rays in the outer heliosphere, Astrophys. J., 249, L71, 1981b.

McKibben, R. B., J. J. O'Gallagher, J. A. Simpson and A. J. Tuzzolino, Preliminary Pioneer 10 intensity gradient of galactic cosmic rays, Astrophys. J.(Letters), 181, L9, 1973.

McKibben, R. B., K. R. Pyle, J. A. Simpson, A. J. Tuzzolino and J. J. O'Gallagher, Cosmic-ray gradients measured by Pioneers 10 and 11, Proc. Int. Cosmic Ray Conf. 14th (Munich), 4, 1512, 1975.

Moraal, H., and L. J. Gleeson, Three-dimensional models of the galactic cosmic-ray modulation, Proc. Int. Cosmic Ray Conf. 14th (Munich), 12, 4189, 1975.

Ng, C. K., Propagation of solar-flare cosmic rays, Ph.D. thesis, Monash University, Melbourne, Australia, 1972.

O'Gallagher, J. J., A time-dependent diffusion-convection model for the long-term modulation of cosmic rays, Astrophys. J., 197, 495, 1975.

O'Gallagher, J. J., and G. A. Maslyar III, A dynamic model for the time evolution of the modulated cosmic-ray spectrum, J. Geophys. Res., 81, 1319, 1976.

Parker, E. N., Cosmic-ray modulation by solar wind, Phys. Rev., 110, 290, 1958.

Parker, E. N., The scattering of charged particles by magnetic irregularities, J. Geophys. Res., 69, 1755, 1964.

Parker, E. N., The passage of energetic charged particles through interplanetary space, Planet. Space Sci., 13, 9, 1965.

Parker, E. N., The effect of adiabatic deceleration on the cosmic ray spectrum in the solar system, Planet. Space Sci., 14, 371, 1966.

Parker, E. N., Cosmic-ray diffusion, energy loss, and the diurnal variation, Planet. Space Sci., 15, 1723, 1967.

Perko, J. S., and L. A. Fisk, Solar modulation of galactic cosmic rays. 5. Time-dependent modulation, J. Geophys. Res., 88, 9033.

Perko, J. S., W. R. Webber and L. A. Fisk, Solar modulation of galactic antiprotons, General Meeting, American Physical Society, April 23-26, 1984, Washington; Bull. Am. Phys. Soc., 29, 705, 1984.

Protheroe, R. J., Cosmic ray antiprotons in the closed galaxy model, Astrophys. J., 251, 387, 1981.

Rygg, T. A., and J. A. Earl, Balloon measurements of cosmic-ray protons and helium over half a solar cycle, 1965-1969, J. Geophys. Res., 76, 7445, 1971.

Tan, L. C., and L. K. Ng, Prediction of interstellar antiproton flux using a nonuniform galactic disk model, Astrophys. J., 269, 751, 1983.

Teegarden, B. J., T. T. von Rosenvinge, F. B. McDonald, J. H. Trainor and W. R. Webber, Measurements of the fluxes of galactic cosmic-ray ^{2}H and ^{3}He in 1972-1973, Astrophys. J., 202, 815, 1975.

Urch, I. H., and L. J. Gleeson, Energy losses of galactic cosmic rays in the interplanetary medium, Astrophys. Space Sci., 20, 177, 1973.

Van Hollebeke, M. A. I., J. R. Wang and F. B. McDonald, The modulation of low-energy galactic cosmic rays, Proc. Int. Cosmic Ray Conf. 13th (Denver), 2, 1298, 1973.

Webb, G. M., W. I. Axford, and M. A. Forman, Cosmic-ray acceleration and transport in stellar winds with terminal shocks, Proc. Int. Cosmic Ray Conf. 18th (Bangalore), 2, 263, 1983.

Webber, W. R., and J. A. Lockwood, A study of the long-term variation and radial gradient of cosmic rays out to 23 AU, J. Geophys. Res., 86, 11458, 1981.

Zwickl, R. D., and W. R. Webber, Solar particle propagation from 1 to 5 AU, Sol. Phys., 54, 457, 1977.